Precipitation Susceptibility in Marine Stratocumulus and Shallow Cumulus from Airborne Measurements

Eunsil Jung[1], Bruce A. Albrecht[1], Armin Sorooshian[2,3], Paquita Zuidema[1], Haflidi H. Jonsson[4]

[1]Department of Atmospheric Sciences, University of Miami, Miami, FL, 33149, United States
[2]Department of Chemical and Environmental Engineering, University of Arizona, Tucson, AZ, 85721, USA
[3]Department of Hydrology and Atmospheric Sciences, University of Arizona, Tucson, AZ, 85721, USA
[4]Naval Postgraduate School, Monterey, CA, 93943, USA

Correspondence to: Eunsil Jung (eunsil.jung@gmail.com)

Abstract. Precipitation tends to decrease as aerosol concentration increases in warm marine boundary layer clouds at fixed liquid water path (LWP). The quantitative nature of this relationship is captured using the precipitation susceptibility (S_o) metric. Previously published works disagree on the qualitative behavior of S_o in marine low clouds: S_o decreases monotonically with increasing LWP or cloud depth (H) in stratocumulus clouds (Sc), while it increases and then decreases in shallow cumulus clouds (Cu). This study uses airborne measurements from four field campaigns on Cu and Sc with similar instrument packages and flight maneuvers to examine if and why S_o behavior varies as a function of cloud type. The findings show that S_o increases with H and then decreases in both Sc and Cu. Possible reasons for why these results differ from those in previous studies of Sc are discussed.

1 Introduction

Cloud-aerosol interactions are considered to be one of the most important forcing mechanisms in the climate system (IPCC, 2013). It is believed that aerosols suppress precipitation in warm boundary layer clouds. However, there is considerable disagreement on the magnitude and even on the sign of how aerosol perturbations affect cloud fraction and lifetime (Stevens and Feingold, 2009). Furthermore, aerosol effects on clouds and precipitation are not readily separable from the effects of meteorology. The precipitation susceptibility metric, S_o, quantifies how aerosol perturbations alter the magnitude of the precipitation rate (R) while minimizing the effects of macrophysical factors (i.e., meteorology) (Feingold and Siebert, 2009). It is defined as

$$S_o = -\frac{d\ln R}{d\ln N_d}, \quad (1)$$

and is evaluated at fixed cloud macrophysical properties, such as cloud thickness (H) or liquid water path (LWP). In Eq. (1), aerosol effects are embedded in the cloud droplet number concentration (N_d) variable since aerosols serve as cloud condensation nuclei (e.g., as aerosol concentration increases, N_d increases). The minus sign is used in Eq. (1) to achieve a positive value of S_o due to the expectation that increasing aerosols reduce precipitation (all else fixed). Towards improving

the representation of precipitation in larger-scale models, the application of Eq. (1) has also been studied using more highly resolved models and remote sensing (e.g., Feingold and Siebert, 2009; Sorooshian et al., 2009; Terai et al., 2015; Hill et al., 2015). In the original work on S_o (Feingold and Siebert, 2009), cloud-base R and N_d were used. Since then, slightly different definitions of S_o have been applied. For example, Sorooshian et al. (2009) used an aerosol proxy (e.g., Aerosol Optical Depth and Aerosol Index) instead of N_d for their satellite data analysis. Terai et al. (2012, 2015) further defined precipitation susceptibility as the sum of the susceptibilities of drizzle intensity (S_I) and drizzle fraction (S_f), $S_R=S_I+S_f$, where S_I is analogous to S_o but calculated exclusively for clouds that produce measurable precipitation. S_I is equivalent to S_o only when 100 % of the sampled clouds are precipitating. Other studies focus on the probability of precipitation (POP), defined as the ratio of the number of precipitating events over the total number of cloudy events. S_{pop} is used in some studies of precipitation susceptibility (e.g., Wang et al., 2012; Mann et al., 2014; Terai et al., 2015), and is equivalent to the S_f used within Terai et al. (2012). In addition to the different definitions of precipitation susceptibility, various forms of R and N_d (e.g., cloud-base, vertically integrated, or ground-based values) with different data thresholds have been used for the calculation of the precipitation susceptibility depending on the data available. In this study, precipitation susceptibility indicates S_o as defined in Eq. (1) unless otherwise stated.

In global climate models (GCMs), aerosol effects on precipitation are represented by either a prognostic scheme or an empirical diagnostic scheme. When GCMs consider aerosols, the rainrate R is often parameterized in terms of LWP and N_d as Eq. (2).

$$R = LWP^{\alpha} N_d^{-\beta}. \quad (2)$$

Climate models typically assume a fixed value of the autoconversion parameter (β in Eq. 2), ranging between approximately 0 and 2 (e.g., Rasch and Kristjansson, 1998; Khairoutdinov and Kogan, 2000; Jones et al., 2001; Rotstayn and Liu, 2005; Takemura et al., 2005). S_o in Eq. (1) is equivalent to the exponent β in Eq. (2) at fixed LWP. Field studies of precipitating stratocumulus (Sc) clouds have reported β values ranging from 0.8 to 1.75 at fixed LWP (e.g., Pawlowska and Brenguier, 2003; Comstock et al., 2004; vanZanten and Stevens, 2005; Lu et al., 2009). However, such single power law fits do not capture the changes in S_o with LWP or H, which is important since previous works have revealed that the response of cloud rainrates to aerosol perturbations vary as a function of LWP (or H).

The qualitative behavior of S_o has been studied for low clouds using models, remote sensing data, and in situ measurements. For model studies of warm cumulus clouds (e.g., the adiabatic parcel model of Feingold and Siebert, 2009), S_o varies from 0.5 to 1.1 with increasing LWP, and exhibits three regimes. At low LWP, not enough water is available with which to initiate rain, and S_o is insensitive to aerosol perturbations. At intermediate LWP, suppression of collision-coalescence by the increased aerosols is most effective. We will refer to this regime as the ascending branch of S_o following Feingold et al. (2013). At high LWP, the precipitation rate is more strongly influenced by the LWP, and S_o decreases with increasing LWP (the descending branch of S_o). This LWP-dependent pattern of S_o is supported by satellite observations

(Sorooshian et al., 2009; 2010) and large-eddy simulations (LES) (Jiang et al., 2010) for warm trade cumulus clouds. In contrast, Terai et al. (2012) showed that S_R monotonically decreased with increasing LWP and H in Sc clouds based on in-situ measurements acquired during the VAMOS Ocean-Cloud-Atmosphere-Land Study-Regional Experiment (VOCALS-REx) field study, while their S_I, similar to S_o in aforementioned studies, did not reveal any significant change with H and maintained a value of ~0.6. These inconsistent results have raised questions of how cloud type impacts behavior of S_o as a function of either H or LWP.

To begin to unravel why differences in the various studies exist, Feingold et al. (2013) showed in modeling studies that the time available for collision-coalescence (t_c) is critical for determining the LWP-dependent behavior of S_o, and may be at least partly responsible for some of the differences. Gettelman et al. (2013) also showed how the microphysical process rates impact S_o in the NCAR Community Atmosphere Model version 5 (CAM5) GCM. They showed that the behavior of S_o with LWP differs between the GCM and the steady-state model of Wood et al., (2009); the values of S_o were constant or decreased with LWP in the steady state model (consistent with Terai et al., 2012; Mann et al., 2014), whereas the GCM S_o behavior was more consistent with Feingold and Siebert (2009), Sorooshian et al. (2009, 2010), Jiang et al. (2010), Feingold et al. (2013), and Hill et al. (2015). Altered microphysical process rates were able to significantly change the magnitudes of S_o, but the qualitative behavior of S_o with LWP remained unchanged (i.e., S_o increases with LWP, peaks at an intermediate LWP then decreases with LWP). More recently, Mann et al. (2014) analyzed 28 days of data from the Azores Atmospheric Radiation Measurement (ARM) Mobile Facility where the prevalent type of clouds are cumulus (20 %), cumulus under stratocumulus (10-30 %) and single-layer stratocumulus (10 %). They showed that S_{pop} slightly decreased with LWP. Terai et al. (2015) estimated precipitation susceptibility (S_I+S_{pop}) in low-level marine stratiform clouds, which included stratus and stratocumulus clouds, using satellite data. The values of S_o in their study generally showed similar behavior to that reported by Mann et al. (2014). Hill et al. (2015) examined how the representation of cloud microphysics in climate model contributes to the behavior of S_o. They found that single-moment schemes produce the largest uncertainty in S_o. Only through increasing the number of prognostic moments (i.e., multi-moment schemes capable of prognosing the rain droplet number as well as mass) could the dependence of S_o on a particular scheme be reduced.

The inconsistent behavior of S_o in previous studies for warm boundary layer clouds motivates the current study. The focus of this paper is to examine and compare the qualitative behavior of S_o in Cu and Sc using similar airborne measurements encompassing four field campaigns. Two were focused on Sc clouds (VOCALS-Rex and the Eastern Pacific Emitted Aerosol Cloud Experiment, Sect. 2.2) and two campaigns targeted Cu clouds (Barbados and Key West Aerosol Cloud Experiments, Sect. 2.3). The strength of these four field campaigns' airborne measurements is that the same research aircraft was deployed with a similar flight strategy and instrument packages, facilitating a comparative analysis. Each of the four field experiments sampled over an area of about 100 × 100 km, and thus, the interrelationships examined are representative of the GCM spatial resolution. Data and methods are discussed in Section 2, followed by results and

discussion in Sections 3 and 4, respectively. The findings are summarized in Section 5. Acronyms used in this study are listed in Table A1 of the Appendix.

2 Data and methods

2.1 TO aircraft

The Center for Interdisciplinary Remotely Piloted Aircraft Studies (CIRPAS) Twin Otter (TO) research aircraft served as the principal platform from which observations for these four experiments were made. During these four deployments, the TO supported similar instrument packages, and performed similar cloud sampling maneuvers, including vertical soundings and level-leg flights below, inside, and above the clouds. Each research flight lasted ~3-4 hours. The TO included the following three *in-situ* probes for characterizing aerosol, cloud, and precipitation size distributions: the Passive Cavity Aerosol Spectrometer Probe (PCASP), Cloud Aerosol Spectrometer (CAS) and Cloud Imaging Probe (CIP), with each resolving particles of diameters 0.1–2.5 μm, 0.6-60 μm and 25-1550 μm, respectively. A zenith-pointing 95-GHz Doppler radar was mounted on top of the aircraft and detected cloud and precipitation structures above the aircraft. Detailed information of the instruments on the TO and flight strategies is provided elsewhere (Zheng et al., 2011; Jung, 2012). All the instruments were operational during the flights analyzed in this study except for the cloud radar, which was not operational during the VOCALS TO flights.

S_o is calculated from Eq. (1) within bins of the cloud thickness H. H was estimated as the height difference between cloud tops and bases. Cloud tops were determined by the cloud radar with a time resolution of 3 Hz and vertical resolution of 24 m (5 m) in height for Cu (Sc). Cloud bases of Cu were determined by the lifting condensation level (LCL) calculated from the average thermodynamic properties of the sub-cloud layer for a given day. The LCL varied little for Cu, for example, during the Barbados Aerosol Cloud Experiment (Sect. 2.3), the LCLs were 653.9±146 m on average from the aircraft measurements, which agreed with the two-year LCL climatology in this region (700±150 m) as documented in Nuijens et al. (2014). Although it is not shown in this study, S_o was also estimated by using the cloud base heights determined from the Cu cloud-base level-leg flights; these results were similar to those based on the sub-cloud LCL.

In stratocumulus clouds, cloud tops are well defined due to the strong capping temperature inversion (see Zheng et al., 2011) and cloud bases vary more than tops (e.g., Fig. 2 of Bretherton et al., 2010). As a result, the way that the cloud-base is determined may affect S_o since the changes in cloud base alternatively can change the cloud thickness. Therefore, we estimate S_o using three different definitions for cloud base. The first method is with LCL calculated from the average thermodynamic properties of the sub-cloud layer (shown as cb-lcl in Fig. 4, same as Cu). For the second and third definitions (cb-local and cb-mean), cloud bases are determined from the lowest heights where the vertical gradients of liquid water contents (LWC) are the greatest from the LWC profiles. The LWC profiles are obtained i) when the aircraft enters the cloud

decks to conduct level legs (cb-local), and ii) from the nearest one or two soundings to the cloud-base level-leg flights. The average height of these two lowest heights (cb-mean, the average of i and ii) is used in this study, along with cb-lcl and cb-local (Fig. 4 later). In general, the heights approximately corresponded to the lowest heights that the liquid water contents (LWC) exceeded 0.01 g m^{-3}. S_o was also estimated by using the heights from the cloud-base level-leg flights as the cloud bases as did for Cu, and the qualitative behavior of S_o was preserved (not shown).

N_d and R were calculated from the drop size distribution (DSD), which is obtained from CAS (forward scattering) and CIP probes during the cloud-base level-leg flights, respectively. The CAS probe acquires data every 10 Hz and then the DSDs at each channel are averaged to 1 Hz. The CIP acquires data every 1 second. The cloud radar samples at 3 Hz and then is averaged to 1 Hz to match the probe data. Therefore, N_d, R and H in Eq. (1) were calculated in 1 s resolution (except for VOCALS-Rex, see Sect. 2.4). The impact of using one-second data on the S_o estimates will be discussed later in Sect. 3.2. R is defined as

$$R = \frac{\pi}{6}\int_{25\mu m}^{1550\mu m} N(D)D^3u(D)dD\,, \tag{3}$$

where $u(D)$ is the fall speed of a drop with diameter D. Three fall speed formulations are used: (1) $u = k_1 r^2$ with $k_1 \approx 1.19\times10^6$ cm^{-1} s^{-1} was used for cloud droplets up to 30 µm radius; (2) $u = k_3 r$ with $k_3 \approx 8\times10^3$ s^{-1} was used for the size range of 40 µm < r < 0.6 mm; and (3) $u = k_2 r^{1/2}$ with $k_2 \approx 2.01\times10^3$ $cm^{1/2}$ s^{-1} for droplets of 0.6 mm < r < 2 mm.

2.2 Stratocumulus cloud field campaigns: VOCALS-Rex and E-PEACE

From October to November 2008, the VAMOS Ocean-Cloud-Atmosphere-Land Study-Regional Experiment (VOCALS-REx) took place over the Southeast Pacific (69°W-86°W, 12°S-31°S), an area extending from the near coastal region of northern Chile and southern Peru to the remote ocean (Zheng et al., 2011; Wood et al., 2011; also see Fig. 1). Three aircraft were deployed during VOCALS from 14 October to 15 November (NSF/NCAR C-130, DOE G-1, CIRPAS TO). The TO sampled more coastal marine stratocumulus decks near 20 °S 72°W (Fig. 1) than the other two planes. Readers should note that the data in Terai et al. (2012) used for their S_R calculations, were also obtained from VOCALS. However, their results were based on NSF/NCAR C-130 flights that sampled cloud decks away from the coastal area (Fig. 1). Wood et al. (2011) provide a comprehensive description of VOCALS experiments and Zheng et al. (2011) provide a description of TO aircraft data during the VOCALS. TO data from flights with decoupled boundary layers, abnormally higher cloud bases, and moist layers above cloud tops were excluded, reducing the total number of flights analyzed to thirteen from the original total of eighteen (Table 1).

From July to August 2011, the Eastern Pacific Emitted Aerosol Cloud Experiment (E-PEACE) took place off the coast of Monterey, California to better understand the response of marine stratocumulus to aerosol perturbations (Russell et al., 2013). E-PEACE included sampling controlled releases of i) smoke from the deck of the research vessel *Point Sur*, and ii) salt aerosol from the TO research aircraft, along with sampling iii) exhaust from container ships transiting across the study area (see Fig. 2 from Russell et al., 2013). During nine out of thirty E-PEACE flights, salt powder (diameter of 1-10 μm) was directly introduced into the cloud decks to examine the effects of giant cloud condensation nuclei (GCCN) on the initiation of warm precipitation (Jung et al., 2015). After excluding the seeding cases and the non-typical Sc decks, 13 flights remained from which we analyzed data (Table 1). Detailed information about E-PEACE and TO data can be found elsewhere (Russell et al., 2013; Wonaschütz et al., 2013).

2.3 Marine cumulus cloud field campaigns: BACEX and KWACEX

Shallow marine cumulus clouds are by far the most frequently observed cloud type over the Earth's oceans, yet remain poorly understood, and have not been investigated as extensively as oceanic stratocumulus. The marine environments in the Caribbean Sea and the Atlantic Ocean provide an excellent area to sample shallow marine cumulus clouds with a high propensity to precipitate. In addition, African dust is transported from westward off of Africa periodically over the North-Atlantic, affecting clouds in its path including around Barbados and Key West, and thus providing an excellent opportunity to observe aerosol-cloud-precipitation interactions. To better understand such interactions in these trade cumuli regimes, the Barbados Aerosol Cloud Experiment (BACEX) was carried out off the Caribbean island of Barbados during mid March and mid April 2010 (Jung et al., 2013), and the Key West Aerosol Cloud Experiment (KWACEX) during May 2012 near Key West (Fig. 1). For the BACEX, we analyzed 12 flights (Table 1). Readers are referred to Jung et al. (2016) for detailed information about the cloud and aerosol properties during the BACEX. The marine atmosphere during KWACEX was dry overall. Six out of 21 flights sampled shallow marine cumulus clouds, of which four had sufficient data for analysis (Table 1).

2.4 S_o calculation details

The distribution of N_d and R, with the corresponding H, is shown in Fig. 2 for each field campaign as scatter diagrams of N_d and R. All data shown in Fig. 2 were obtained during the cloud-base level-leg flights. The Southeast Pacific (SEP) Sc decks (VOCALS, Fig. 2a) were overall drier and more polluted than those in the Northeast Pacific (NEP) Sc decks (E-PEACE, Fig. 2c); R=0.03 mm day^{-1} (median) and N_d=232 cm^{-3} in VOCALS, but R=1.04 mm day^{-1} and N_d=133 cm^{-3} in E-PEACE. During E-PEACE, high N_d was observed in a few cases, (e.g., N_d > 400 cm^{-3} in Fig. 2c), and they were likely associated with the emitted aerosols from the ship exhaust and smoke (Russell et al., 2013; Wang et al., 2014; Sorooshian et al., 2015). The marine environments of the Caribbean Seas showed wide variations of R (e.g., order of 10^{-2} to 10^{2} mm day^{-1};

Fig. 2b and Fig. 2d). The Barbados campaign sampled the most pristine environment of the four campaigns (N_d < 350 cm^{-3}, N_d = 61 cm^{-3} on average), reflecting the isolated location of the island in the North Atlantic even though the experiment period included the most intense dust events of 2010 (Jung et al., 2013). The marine environment near Key West was more polluted than Barbados throughout the KWACEX campaign (Fig. 2d, N_d = 206 cm^{-3} on average).

S_o was about 0.62 for E-PEACE (linear regression correlation coefficient r=0.34), if calculated using all the individual 1 Hz data points shown in Fig. 2 where H ranges from ~100 m to 500 m. However, S_o was about 0.42 (r=0.21) if one rainy day (shown as double circles in Fig. 10 later) was excluded from the analysis, suggesting the artifact of wet scavenging (see Sect. 4), a different predominant cloud microphysical process (auto-conversion versus accretion) or the influence of macrophysical properties other than H. These E-PEACE S_o values agree with values estimated in previous campaigns in the same northeast Pacific region for H ~200-600 m: S_o ~0.46-0.48 using H and S_o ~0.60-0.63 using LWP (Lu et al., 2009). S_o during VOCALS is about 1.07 (r=0.46) for H ~ 150-700 m. Overall, S_o values in this study are within the range of S_o from the previous field studies of precipitating stratocumulus clouds (S_o ~0.8 to 1.75 for a fixed LWP in the studies of Pawlowska and Brenguier, 2003; Comstock et al., 2004; vanZanten and Stevens, 2005). Values of S_o for BACEX and KWACEX are about 0.89 (r=0.38) and 0.77 (r=0.39), respectively.

Although single power law fits for a given field campaign give the general sense of S_o values, they do not show the qualitative behavior of S_o with H, which reveals which thickness is most susceptible to aerosol perturbations. To further examine this, S_o is calculated by assigning R and N_d into the given intervals of cloud thickness for each campaign. The width of each H interval is taken to be 30 m for Sc and 50 m for Cu. The H intervals are arbitrary, but chosen to contain a similar number of data points within each interval and provide a robust S_o regardless of the interval choice. Within each H interval, we performed a linear regression to find a best fit for the natural log of the precipitation rate against natural log of N_d, and the S_o is the slope of the fit (see Fig. 3, Fig. 6, for example). Cloud data are included in the analysis if the given precipitation rate is greater than a threshold of 0.001 mm day^{-1}. The low R threshold is intended to include both non-precipitating and precipitating clouds. The impacts of the R threshold and H intervals on the S_o estimates are discussed in Appendix B and C, respectively. An example of S_o is shown in Fig. 3 from E-PEACE using every 1-second cloud data point (i.e., N_d and R) for H between 160 m and 190 m. The slope (i.e., linear fit) in Fig. 3 corresponds to an S_o value of 0.24. The value of S_o (0.24) is then plotted in the corresponding H on the H- S_o diagram (e.g., Fig. 4 at the H of 174 m, which corresponds to the average H of the interval). The same procedure is repeated for all H intervals to obtain the complete pattern of S_o with H. We tested and applied a few criteria in the S_o calculations, such as minimum R thresholds, and the total number of cloud data points and spans of N_d for a given H interval. Based on these sensitivity tests, we calculated S_o exclusively if N_d varied a sufficient amount (e.g., dln(N_d) spans at least 2.2) for a given H interval since little variation of N_d does not provide the proper perturbation of aerosols. For example, in Fig. 3a, dln(N_d) spans about 3.5. Slightly different and broader criteria were applied for Cu mainly due to the larger number of data points sampled in Sc. However, the qualitative behavior of S_o was robust as

long as the variation of N_d was sufficiently large, regardless of the other criteria, although the details were different (e.g., Fig. B1). Most of the slopes are statistically significant at the 99 % confidence level (e.g., filled symbols in Fig. 4). The number of data points used to calculate S_o and the linear correlations and the P-values indicating the statistically significant level of confidence for the fitted lines are summarized in Table A2 for given H intervals. Additionally, S_o is calculated by considering e-folding time and by randomly resampling the flights (Sect. 3.2), and the results are robust. This will be discussed later.

S_o during VOCALS is calculated in slightly different ways from other experiments since the cloud radar failed. First, H is estimated from the vertical structure of LWC for each day (daily mean H). Once H is determined for each flight, it is assigned to a certain H bin. For example, H of 9 Nov. (164±18 m) and 10 Nov. (194±21 m) are similar and thus assigned to the same H bin (i.e., group 1 in Table 1). VOCALS-H is classified into four distinct groups. Once N_d and R are assigned to the corresponding H, S_o then is estimated by using all the data points that are assigned to the H group.

LWP is commonly used as the macrophysical factor when quantifying Eq. (1). However, in this study, we use H as a macrophysical factor since we aim to compare S_o for both Sc and Cu. H corresponds well to LWP for adiabatic clouds, for which LWP ~ H^2. The adiabatic assumption, which may be valid in Sc, is not valid in Cu (Rauber et al., 2007; Jung et al., 2016) to calculate LWP. Further, even if we calculate LWP by integrating LWC with height (e.g., in Sc), we would obtain one LWP value for the entire cloud layer on a given day, as opposed to many H estimated from the cloud radar sampling at 3 Hz. Moreover, the TO did not carry an instrument that measures LWP directly such as a G-band Vapor Radiometer (e.g., Zuidema et al., 2012). Consequently, the direct comparison with previous results of S_o with LWP (e.g., quantitative) is not possible. We also note that LWC decreases as drizzle rates increase (e.g., see Fig. 8d of Jung et al., 2015). Consequently, clouds that are precipitating (higher R) may have a LWP that is lower than the adiabatic value, and a cloud with a small R may have a LWP close to the adiabatic value. It should be also noted that the ranges of H (and possibly LWP) differ substantially between Cu and Sc. For example, H of Cu in this study can be as high as 1700 m, whereas H of Sc is generally less than 500 m (e.g., Fig. 4). Additionally, H for clouds that begin to precipitate may differ in Sc and Cu. Further, the LWP for clouds that precipitate would be sub-adiabatic and would have a smaller value of LWP than the LWP for non-precipitating clouds. Consequently, S_o that is calculated from cloud fields with diverse cloud types (e.g., Mann et al., 2014; Terai et al., 2015) may be complicated since LWP is shifted to smaller values for (heavily) precipitating clouds, and the H at precipitation initiation may differ between cloud types. In general, the results are used with caution when comparing with other studies in quantifying S_o since the dominating cloud process and the choices applied in how to calculate parameters involved with Eq. (1) can differ widely (e.g., Duong et al., 2011).

3 Results

3.1 S_o in Sc and Cu

In this section, we show S_o calculated in three different ways. First, S_o is calculated with 1-second data (Fig. 4) for BACEX, KWACEX, E-PEACE and VOCALS. Second, S_o is calculated with reduced data points that are averaged over the e-folding time of N_d. We show the results for BACEX, E-PEACE and VOCALS (Figs. 5 and 6). Lastly, S_o is calculated with randomly resampled E-PEACE flights (Figs. 8 and 9). We will show the results in turns.

S_o as a function of H is shown in Fig. 4a for Cu. S_o is calculated from Eq. (1) with N_d and R that are sampled during the cloud-base level-leg flights at 1-second resolution. Cloud level-leg flights usually last 7-15 minutes on average, with an aircraft speed of 50-60 m s^{-1}. In Fig. 4a, S_o during BACEX fluctuates around zero for clouds shallower than 500-600 m, above which S_o begins to increase rapidly with a peak of ~1.6 near H~1400 m. After that, S_o starts to decrease as H increases. The S_o during KWACEX follows S_0 from BACEX, especially in the thicker cloud regime where the majority of KWACEX data were sampled.

The qualitative behavior of S_o for Sc is shown in Fig. 4b. S_o during E-PEACE shows H-dependent S_o patterns that are similar to those from BACEX. In the small H regime (H < 240 m), S_o is almost constant at ~0.2. For H > ~240 m, S_o increases gradually with increasing H and peaks at S_o ~ 1.0 near H ~ 350-400 m. After that, S_o decreases with increasing H. Figure 4b further shows that the overall pattern of S_o is similar regardless of how the cloud bases were determined, although the H at which S_o peaks changes slightly (cb-mean, cb-local, cb-lcl).

During VOCALS, S_o increases with increasing H, from S_o ~0.1 near 170 m to S_o ~0.5 near 300 m. A minimum S_o value is shown near H ~ 640 m. The negative values of S_o in the largest H regime possibly result from uncertainties in the S_o estimation or in unaccounted-for macrophysical properties, such as, cloud lifetime. The failure of the cloud radar during VOCALS was responsible for the fewer (four) H groups (Table 1). Additionally, no data were available for H ~ 350-600 m (Fig. 3), and thus, it is possible that S_o peaks anywhere between H values of 300 m and 600 m. The results of VOCALS clearly show the disadvantage of no cloud radar (i.e., high resolution of LWP or H) for the S_o estimates.

3.2 S_o calculated with an e-folding time and randomly resampled flights.

The dependence of 1-second data (N_d, R) on each other is tested two ways. First, we calculated S_o by considering the e-folding time scale (Leith, 1973), and, secondly, we calculated S_o by randomly resampling the flights. The e-folding time of N_d during E-PEACE was found to vary from four minutes to ten minutes, while the e-folding time of R varied from a few seconds to one to two minutes. The e-folding time of N_d within the VOCALS-TO flights varied from two to six minutes, and for the cloud-base precipitation was less than (or approximately) 1 minute (for a horizontal distance of less than 3 km, consistent with Terai et al., 2012). In the case of BACEX (Cu), the overall e-folding times were much shorter, varying from

one-two minutes for N_d and less than one. The e-folding times of N_d and R are summarized in Table 1 for VOCALS, E-PEACE and BACEX. KWACEX was not included since there were only four flights.

We calculated S_o with data averaged over the upper bounds of the e-folding time (i.e., e-folding time of N_d) for E-PEACE, BACEX and VOCALS flights, and the qualitative behaviour of S_o reported with 1-second data is unchanged: S_o increases with H then peaks before it decreases again (Fig. 5 for BACEX and E-PEACE and Fig. 6 for VOCALS). However, it should be noted that the H that S_o peaks at is shifted toward the lower H consistent with the results of Duong et al. (2011). The shift of H to the lower H is substantial in Sc where the overall H is smaller than H of Cu. Additionally, the effect of the H-interval on the S_o estimates is discussed in Appendix C. In general, the results are robust regardless of the H interval. However, if the H interval is chosen across a cloud thickness range in which S_o changes substantially, the pattern of S_o can be changed, indicating that the finer H interval provide a more accurate S_o variation.

Second, we estimated S_o by randomly resampling the flights of E-PEACE to see whether the sequential 1-second samples are statistically independent. S_o calculated with random flights, at first glance, showed two distinctive types of behavior (not shown, but similar to Fig. 8a shown later). One is a similar pattern to that of the current S_o shown in Fig. 4 while the other is an almost constant S_o near zero. The cloud data sampled during E-PEACE formed two groups (denoted as A and B in Figure 7). The S_o pattern calculated with cloud data of group A is similar to S_o shown in Fig. 4: S_o is constant at lower H, followed by increase then decrease (Fig. 8a). In contrast, S_o values calculated from group B were relatively constant near zero S_o with the descending branch only (blue in Fig. 8c). Further analysis revealed that the two RFs (RF13 and RF03) that have relatively small N_d with high R explain the differences in the S_o patterns (Fig. 9). If S_o is calculated with cloud data that do not include data from clean with heavy precipitating environments (i.e., RF13 and RF03), S_o shows a similar pattern as that in Fig. 4.

3.3 The effect of autoconversion and accretion processes on S_o

For cloud droplets to become raindrops (typical diameters of cloud droplets and drizzle drops are about 20 and 200 μm, respectively (Rogers and Yau, 1989)), they have to increase in size significantly by the collision-coalescence process (autoconversion and accretion) Here, autoconversion primarily refers to faster-falling large cloud droplets that collect smaller cloud droplets in their paths as they fall through a cloud and grow larger; accretion refers to precipitation embryos that collect cloud droplets. In the intermediate LWP regime where S_o increases with LWP or H (ascending branch of S_o) the auto-conversion process dominates. On the other hand, in the high LWP regime where S_o decreases with LWP or H (descending branch of S_o) the accretion process dominates (Feingold and Siebert, 2009; Feingold et al., 2013). The transition from the dominance of autoconversion to accretion is reported to occur when D_e exceeds ~ 28 μm, and has been used as a rain initiation threshold in Sc (e.g., Rosenfeld et al., 2012). Jung et al. (2015) also showed that the precipitation embryos

appeared (and warm rain initiated) when the mean droplets diameters were slightly less than 30 μm from the salt seeding experiments during E-PEACE, in the NEP Sc decks (e.g., see Table 3, Fig. 6a, and Fig. 7 in their study). Figure 10(a) shows that clouds during VOCALS consisted of numerous small droplets (D < 15 μm in Fig. 5a), which primarily are involved with the autoconversion process except for one flight (D ~37 μm, RF09, Nov. 1). The dominance of smaller droplets during VOCALS-TO flights agree with the dominance of ascending branch of S_o in Fig. 4(b). On the other hand, E-PEACE Sc clouds are composed of larger-sized droplets as well as small droplets (Fig. 10b).

4 Discussion

This study shows the consistent behavior of S_o as a function of a key macrophysical cloud property regardless of cloud type; i.e., S_o increases with increasing H (ascending branch) and peaks at intermediate H before S_o decreases with H (descending branch) in both Sc and Cu (Fig. 4). The results from marine cumulus clouds (BACEX and KWACEX) are consistent with previous modeling and observational studies of warm cumulus clouds (Sorooshian et al., 2009, 2010; Jiang et al., 2010; Duong et al., 2011; Feingold and Siebert, 2009; Feingold et al., 2013). However, S_o values estimated from marine stratocumulus clouds (E-PEACE and VOCALS) are inconsistent with previous in-situ observations of warm stratocumulus clouds (Terai et al., 2012; Mann et al., 2014), but are consistent with previous satellite observations of weakly precipitating Sc (Sorooshian et al., 2010), global climate model simulations (Gettelman et al., 2013; Hill et al., 2015), and box and parcel model studies (Feingold et al., 2013) of Sc.

Possible reasons for why the current results differ from those in previous studies of Sc are discussed here mainly by comparing results to those from the Terai et al. (2012) study. The inconsistent behaviors of S_o between our study and theirs may be due to a number of factors. One of the most fundamental reasons could be in the differences in the cloud fields that were sampled. In the SEP Sc decks, drizzle intensity and frequency tend to increase westward from the coast (e.g., Bretherton et al., 2010) and their dataset included several Pockets of Open Cells (POCs) with strong precipitation (personal communication with C. Terai). It should be noted that the VOCALS C130 flights (Terai et al., 2012) sampled the cloud fields along 20 °S (mainly over the open Ocean), whereas the VOCALS TO flights sampled the Sc decks near the continents (Fig. 1). The westward increases in frequency and intensity of drizzle coincident with the westward decrease in aerosols and N_d, and also with larger LWP over the open ocean (e.g., Zuidema et al. 2012), suggesting that the discrepancy possibly is contributed to the different cloud microphysical process working on the cloud field (auto-conversion versus accretion processes). Indeed, Gettelman et al. (2013) showed that the accretion process dominated during VOCALS C-130 flights; the accretion to autoconversion ratio was above 1 for all LWP ranges during VOCALS observation (e.g., Fig. 5a in their studies). Therefore, the enhanced (major) accretion process appears as a descending branch of S_o predominantly. Hill et al.

(2015) also showed that the monotonic decrease of S_o with LWP in case that the cloud data consist of exclusively larger particles (e.g., radius > 20 μm)

Second, the higher R threshold that Terai et al. (2012) used could contribute to the discrepancies. Terai et al. (2012) used R = 0.14 mm day^{-1} as a minimum R threshold to estimate S_o where 0.14 mm day^{-1} corresponds to -15 dBz from the Z-R relationship that they used (R=2.01$Z^{0.77}$ from Comstock et al., 2004). This R threshold is possibly too high to capture the autoconversion processes that occur in more lightly precipitating clouds such as clouds sampled during VOCALS TO flights. As a result, the high value of minimum R threshold may primarily capture the accretion process, which may contribute to the descending branch of S_o in their study. As an example, this R threshold rejects all the data in Fig. 2a (VOCALS TO flights) except for one day (RF09, Nov. 1) when the mean effective diameter is about 37 μm and the accretion process dominates for the day. Further, the impact of the R threshold on the S_o estimates is evident in Fig. B2. Figure B2 shows that S_o decreases as the larger minimum R threshold is used, in particular at larger H. Figure 9 also shows how clouds of low N_d with high R (e.g., RF03 and RF13 of E-PEACE) alter the behavior of S_o. The choice of minimum R threshold can change the dataset that will be used for the estimates of S_o. The S_o metric is designed to show the impact of aerosols on precipitation; as aerosol increases, smaller sizes of numerous droplets form, and those droplets suppress the collision-coalescence process, and in turn, precipitation. Therefore, to study the extent that aerosols suppress precipitation, it would be more appropriate to encompass the full range of non-precipitating to precipitating clouds that include both autoconversion and accretion processes. It is also noted that the framework of precipitation susceptibility is to measure the impact of aerosol perturbations on the precipitation suppression, and thus, the concept of S_o may not adequately apply to the clouds that are already heavily precipitating since the accretion process has little dependence on N_d. In addition to decreasing the LWP, the precipitation itself can scavenge aerosols leading to lower N_d.

Third, the overall high values shown in Terai et al. (2012) (S_o begins with around 3 near H~50 m and ends with S_o ~0.8 near H~500 m) may reflect the effects of wet scavenging (Fig. 7a; see also Duong et al., 2011), especially by considering that their dataset included several POCs with strong precipitation. We also noted that S_o calculated from the 13 E-PEACE flights was about 0.62. However, S_o calculated from 12 E-PEACE flights that excluded one rainy day was about 0.42, which is consistent with larger S_o in the presence of (heavy) precipitation possibly due to the wet scavenging (but it is also possible the lower S_o is due to the microphysical process). Consistently, S_o values calculated from 9 BACEX flights (Cu), which excluded three heavy precipitation cases, were also shifted to lower values than those estimated from the entire 13 flights (not shown).

Fourth, Terai et al. (2012) used column-maximum Z and then converted the Z to R by using a Z-R relationship for those time periods when the lidar could not determine the cloud-base height due to interference from heavy precipitation. This procedure can overestimate precipitation for a given N_d. If the procedure (i.e., overestimates of R) occurs in a low N_d regime (left half of the dotted line in Fig. 7b), the steeper slope (i.e., higher S_o) would be obtained (Fig. 7b). If the procedure

happens in a high N_d regime, the lower slope would be attained (Fig. 7c). Based on Fig. 1 of their study, the former scenario (Fig. 7b) would occur, resulting in higher S_o than expected.

Fifth, the Z-R relationship that Terai et al. (2012) used (R=2.01$Z^{0.77}$, followed Comstock et al. (2004)'s Z=25$R^{1.3}$) was derived for stratocumulus off of the coast of Peru, using a shipboard scanning C-band radar. The Sc sampled during the VOCALS C-130 flights may have a different microphysical process from which the original Z-R relationship was derived. The microphysical processes are responsible for the formation of DSD, and the variability of DSD determines the theoretical limit of precipitation accuracy by radar via Z-R relationship. That being said, changes in DSD imply different Z-R relationships. The DSD variability (e.g., day to day, within a day, between physical processes and within a physical process) causes about 30-50 % of errors in R estimates with a single Z-R relationship (e.g., see Lee and Zawadzki, 2005 and references therein). Besides, the Comstock et al. (2004) Z-R relationship was derived from drop-sizes ranged from 2 μm to 800 μm in diameter (for drops larger than 800 μm, extrapolation was used). The Sc from VOCALS C-130 flights included several POCs, while the clouds that the Z-R relationship was derived were characterized by persistent Sc, sometimes continuous and other times broken with intermittent drizzle throughout. Therefore, using the Z-R relationship of Comstock et al. (2004) may result in some additional uncertainties in R estimates in Terai et al. (2012) as the error of Z-R relationship becomes larger in the bigger drop sizes (Z and R are proportional to ~D^6 and ~D^4, respectively). Further, applying a Z-R relationship to W-band (3 mm) radar returns is not valid if there are any droplets greater than 1 mm since non-Rayleigh scattering (Mie effects) can dominate the radar reflectivity. Note that the Terai et al. (2012) R retrievals were made with a W-band radar. However, it is also true that the in-situ sampling of rain used in this study may miss a lot of raindrops because of the small sample volume of the probe. The errors in R estimates with a single Z-R relationship or R measured from probes, however, may not critically affect the differences in S_o between studies as the S_o metric (Eq. 1) is less sensitive to data uncertainty by using the logarithmic form of the data.

Lastly, Terai estimated N_d from the sub-cloud aerosols using an empirical relationship, which may also contribute to the differences. According to Jung (2012 in Fig. 4.5), the sub-cloud aerosols well represent the cloud-base N_d in the updraft regime, although these results are shown for the marine shallow cumulus clouds. Similarly, using the aerosol proxy from the satellite data for the S_o calculation also needs caution. Jung et al. (2016) showed that Aerosol optical depth (AOD) is not always a good indicator of the sub-cloud layer aerosols especially when the fine particles from long-distance continental pollution plumes reside above the boundary layer (e.g., Fig 4-5 their study). Mann et al. (2014) used a sub-cloud 10 m CCN (at 0.55 % super-saturation) for the S_o calculation and showed a decreasing trend of S_o with LWP as Terai et al. (2012) but their overall S_o is smaller than those estimated from other field studies. In cases where sub-cloud aerosols are used for the S_o estimates, these estimates give a smaller S_o than those using N_d due to the decreasing fraction of aerosol activated with N_a increasing, all else being equal (e.g., Lu et al., 2009).

5 Conclusions

The suppression of precipitation due to the enhanced aerosol concentrations (N_a) is a general feature of warm clouds. In this study we examined precipitation susceptibility S_o in marine low clouds by using in situ data obtained from four field campaigns with similar datasets; two of them focused on marine stratocumulus (Sc), and two targeted shallow cumulus (Cu) clouds. We estimate S_o with 1-second data, with data averaged over an e-folding time scale, and data subsampled randomly from flights, with the key results preserved regardless of the method used. This study shows that the maximum values of S_o are ~1.0 for Sc and ~1.5 for Cu, which are less than the values of S_o of ~2.0 that climate models tend to use for the value of $-\beta$ in Eq. 2. This study is the first to show with airborne data that for both Sc and Cu, S_o increases with increasing cloud thickness H and peaks at an intermediate H, before decreasing. For example, R is most susceptible for clouds of medium-deep depth, such as H ~380 m for Sc in NEP where H varies between 100-450 m, and H~1200-1400 m for Cu in the Caribbean Sea where H ranges from 200-1600 m. On the other hand, R is less susceptible to N_d in both shallow non-precipitating and deep heavily precipitating cloud regimes for both Sc and Cu. The results are consistent with previous studies of warm cumulus clouds, but inconsistent with those of warm marine stratocumulus clouds in-situ observations.

We suggest several possible reasons for why these results differ from those in previous studies of Sc, for example, by comparing with in-situ measurements of Terai et al. (2012). The sources of these uncertainties include the following: (i) geographical location of cloud decks that may be related to the predominant cloud microphysical process at work (e.g., accretion process), (ii) R threshold differences, (iii) wet scavenging effects (causing high values of S_o), (iv) the use of maximum column Z to convert R under heavy rain conditions where cloud-base is not defined, (v) the use of the Z-R relationship to estimate R, and (vi) the use of sub-cloud aerosols to estimate cloud-base N_d.

We also found that the details of N_d (e.g., Fig. B1) or how the cloud base is determined have little effect on both S_o values and the qualitative H-dependent behavior (Fig. 4). Further, here we emphasize and caution that the choice of the R threshold for the data analysis is important because the chosen threshold possibly can alter the character of the dataset used to calculate S_o by subsampling the data. For example, if a high value of the minimum R threshold is chosen in a dataset where the majority of data have low precipitation (e.g., VOCALS TO flights, Fig. 3a) and/or in the bimodal population of precipitation, the threshold would, by chance, eliminate/reduce the influence of the autoconversion process in favor of the accretion process. The VOCALS C-130 flight datasets are likely dominated by the accretion process occurring naturally (geographically remote ocean areas where POCs is often observed) and by the choice of high R thresholds.

The values of S_o in this study were calculated from in-situ measurements, and thus, no issues associated with the retrieval (e.g., satellite data), empirical relationships (e.g., Z-R relationship), or assumptions (e.g., relations between sub-cloud aerosols and cloud-base N_d) are encountered for the calculation of S_o. A drawback, however, is the much smaller sampling volume of the in-situ microphysical probes compared to a radar volume, as this may generate an underestimate of the rainrate. Further, we calculated S_o separately for Cu and Sc to avoid any possible issues that may arise from combining

different cloud types (Sect. 2.4). The results, however, should be used with caution when comparing to other studies in quantifying S_o as the dominating cloud process and the choices applied to calculate the parameters in S_o estimates (Eq. 1) can differ widely.

The results of this work motivate future studies examining the same relationships with a more direct measurement of cloud depth using a cloud radar and/or LWP using a microwave radiometer, in addition to the instruments/sensors that measure/retrieve R and N_d (N_a is also desirable). For the flight strategy, in-cloud level legs at multiple altitudes (cloud-base, mid-cloud and cloud-top) with one sub-cloud level-leg would be ideal to calculate S_o and compare with other studies where S_o is calculated with cloud-base or vertically integrated variables. Level-legs near the ocean surface and sounding(s) to examine the background thermodynamic structures on a given day are also recommended.

5 Data availability

The Twin Otter research aircraft dataset are available from upon request by email at balbrecht@rsmas.miami.edu or ejung@rsmas.miami.edu.

Appendix A: Data

Table A1. Table of acronyms and symbols.

Acronym	Expression
BACEX	Barbados Aerosol Cloud Experiment
CAS	Cloud Aerosol Spectrometer
CIP	Cloud Imaging Probe
Cu	(Shallow marine) Cumulus (cloud)
DSD	Drop Size Distribution
E-PEACE	Eastern Pacific Emitted Aerosol Cloud Experiment
H	Cloud thickness
KWACEX	Key West Aerosol Cloud Experiment
LCL	Lifting Condensation Level
LWC	Liquid Water Content
LWP	Liquid water path
N_d	Cloud droplet number concentration
PCASP	Passive Cavity Aerosol Spectrometer Probe
POCs	Pockets of Open Cells
R	Rainfall (Precipitation) Rate
Sc	Stratocumulus (clouds)
S_o	Precipitation susceptibility
TO	Twin Otter
VOCALS-REx	VAMOS Ocean-Cloud-Atmosphere-Land Study-Regional Experiment
Z	Radar reflectivity

Table A2. H interval and number of data points used in Fig. 4 for each field study.

E-PEACE, H (m)	H < 130	130-160	160-190	190-220	220-250	250-280	280-310	310-340	340-370	370-400	400-430	*H*>430
E-PEACE (cb-mean) (#, *r*, *P*)	537 *r*=0.03 *P*=0.548	499 *r*=0.13 ***P*=0.0025**	444 *r*=0.16 ***P*=0.0006**	508 *r*=0.16 ***P*=0.0004**	886 *r*=0.13 ***P*=0.0001**	781 *r*=0.27 ***P*<0.00001**	606 *r*=0.41 ***P*<0.00001**	610 *r*=0.50 ***P*<0.00001**	821 *r*=0.58 ***P*<0.00001**	373 *r*=0.74 ***P*<0.00001**	97 *r*=0.43 ***P*<0.0001**	10 *r*=0.05 *P*=0.89
E-PEACE (cb-local) (#, *r*, *P*)	530 *r*=0.07 *P*=0.09	482 *r*=0.14 ***P*=0.0029**	582 *r*=0.11 ***P*=0.0076**	683 *r*=0.12 ***P*=0.0015**	726 *r*=0.14 ***P*=0.0002**	474 *r*=0.20 ***P*<0.00001**	497 *r*=0.44 ***P*<0.00001**	525 *r*=0.48 ***P*<0.00001**	602 *r*=0.51 ***P*<0.00001**	758 *r*=0.62 ***P*<0.00001**	236 *r*=0.77 ***P*<0.00001**	77 *r*=0.56 ***P*<0.00001**
E-PEACE (cb-lcl) (#, *r*, *P*)	514 *r*=0.03 *P*=0.46	379 *r*=0.07 *P*=0.19	341 *r*=0.10 *P*=0.067	255 *r*=0.10 *P*=0.102	489 *r*=0.17 ***P*=0.0002**	823 *r*=0.20 ***P*<0.00001**	627 *r*=0.36 ***P*<0.00001**	621 *r*=0.45 ***P*<0.00001**	670 *r*=0.54 ***P*<0.00001**	389 *r*=0.46 ***P*<0.00001**	283 *r*=0.02 *P*=0.782	781 *r*=0.05 *P*=0.174
VOCALS H (m)	Group1 170±27	Group 2 225±46	Group 3 307±24	Group 4 641±201	-	-	-	-	-	-	-	-
VOCALS (#, *r*, *P*)	1113 *r*=0.04 *P*=0.161	1280 *r*=0.27 ***P*<0.00001**	833 *r*=0.45 ***P*<0.00001**	224 *r*=0.14 *P*=0.042	-	-	-	-	-	-	-	-
BACEX H (m)	0-250	250-500	500-600	600-800	800-1000	1000-1250	1250-1500	*H*>1500	-	-	-	-
BACEX (#, *r*, *P*)	23 *r*=0.03 *P*=0.88	89 *r*=0.03 *P*=0.76	46 *r*=0.29 *P*=0.05	87 *r*=0.12 *P*=0.25	52 *r*=0.60 ***P*<0.00001**	37 *r*=0.58 ***P*=0.0002**	30 *r*=0.59 ***P*=0.0006**	27 *r*=0.52 ***P*=0.005**	-	-	-	-
KWACE XH (m)	*H*<1500	1500-1800	*H* > 1800	-	-	-	-	-	-	-	-	-
KWACE X (#, *r*, *P*)	56 *r*=0.23 *P*=0.095	32 *r*=0.52 ***P*=0.002**	42 *r*=0.16 *P*=0.32	-	-	-	-	-	-	-	-	-

Numbers indicates that the total number of data points, followed by the linear regression correlation coefficient (*r*) and P-value (two-tailed t-test).
Bold P-values indicate that correlations are statistically significant at the 99% confidence level.

Appendix B: Sensitivity of R and N_d thresholds to S_o estimates

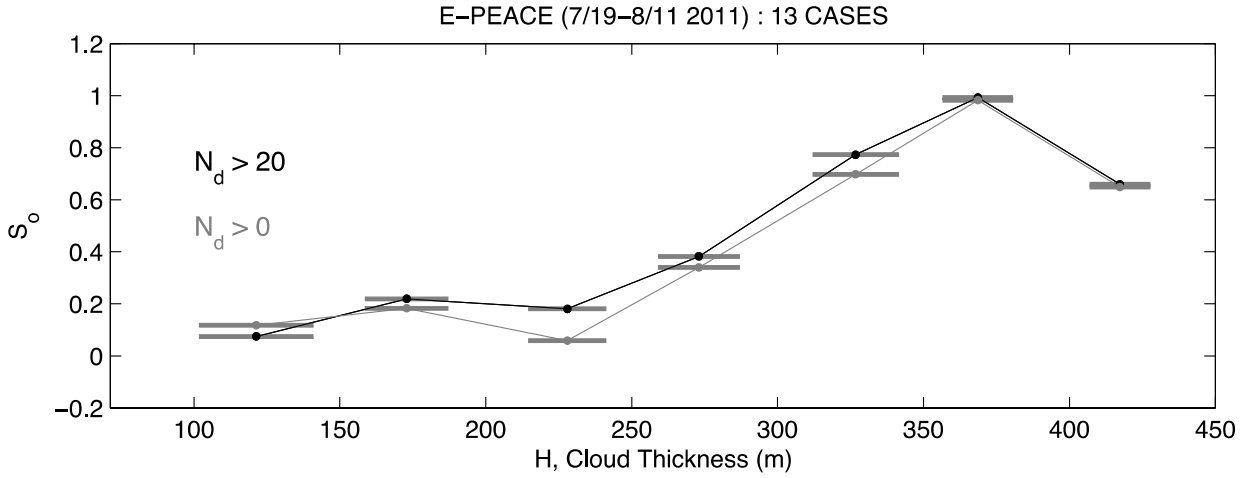

Figure B1. The sensitivity of S_o to N_d threshold values. One standard deviation of mean thickness for given H intervals are shown as horizontal bars.

5

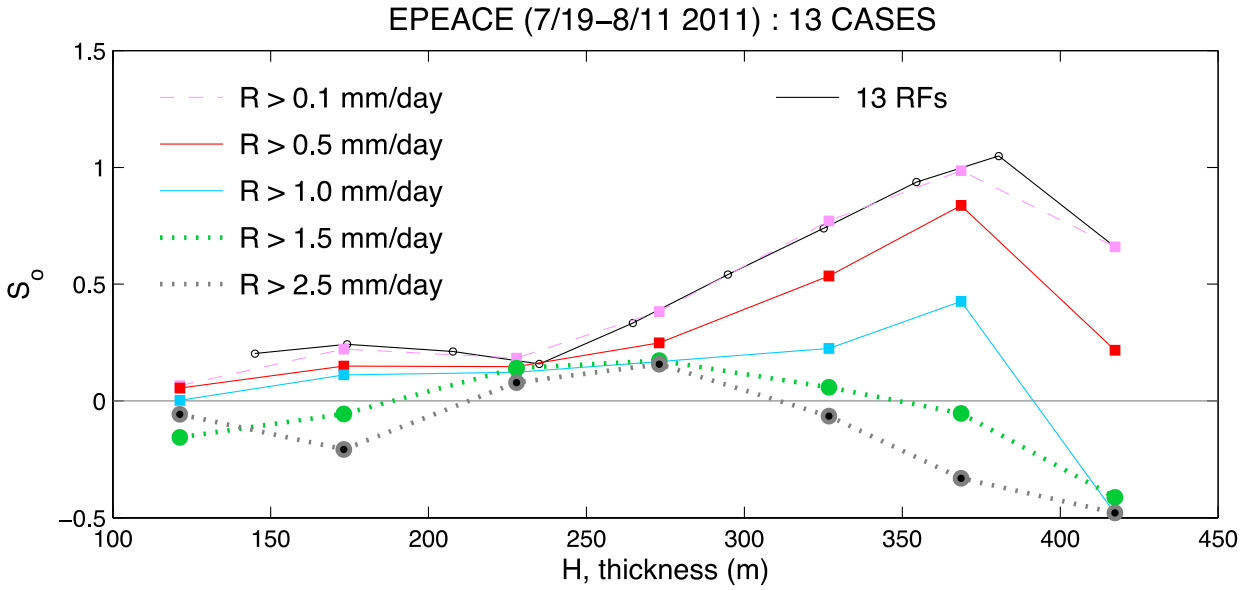

Figure B2. H-dependent precipitation susceptibility as a function of R threshold values.

10

Appendix C. The effect of *H* intervals on S_o estimates.

S_o calculated with different H intervals can be seen by comparing Fig. 4 and Fig. A1 as an example. H intervals in Fig. 4(b) are about 30 m, while H intervals in Fig. A1 are about 50 m. The qualitative H-dependent behavior of S_o is robust regardless of the chosen H intervals in case 1-second data are used. However, the chosen H interval may have effect on the estimate of S_o that is calculated with a fewer data points, such as S_o that is calculated with data averaged over the e-folding time.

The effect of H-intervals on S_o estimates, which is estimated with data averaged over the e-folding time, is shown in Fig. B1. In summary, the results are robust regardless of H interval in general. However, if the H interval is chosen across the cloud thickness where the S_o changes substantially (such as in which the cloud properties change substantially), the pattern of S_o can be changed, indicating that the finer H interval would provide more accurate S_o. This is shown in Figs. 7 and 8. In Fig. 7, an H interval of 50 m hides the variation of S_o between H 150 m and 200 m. The ln (N_d) and –ln(R) diagrams for H widths of 40 am nd 50 m are shown in Fig. 7. However, in case that the S_o does not change substantially across the H intervals, the S_o does not change even if the larger H interval is used (e.g., Fig. 8d). For example, S_o calculated with subsets of data (e.g., $220 \leq H < 250$ m, $250 \leq H < 280$ m, $280 \leq H < 310$ m) are about ~ 0.24 to 0.25. If the S_o is estimated with all the data that fall into the three intervals (e.g., $H > 200$ m), the value is about 0.28, which is similar to three individual S_o values. The results may indicate that the cloud properties such as cloud thickness where the cloud begins to precipitate could be of importance for accurate estimates of S_o by affecting the optimal H interval and/or ranges.

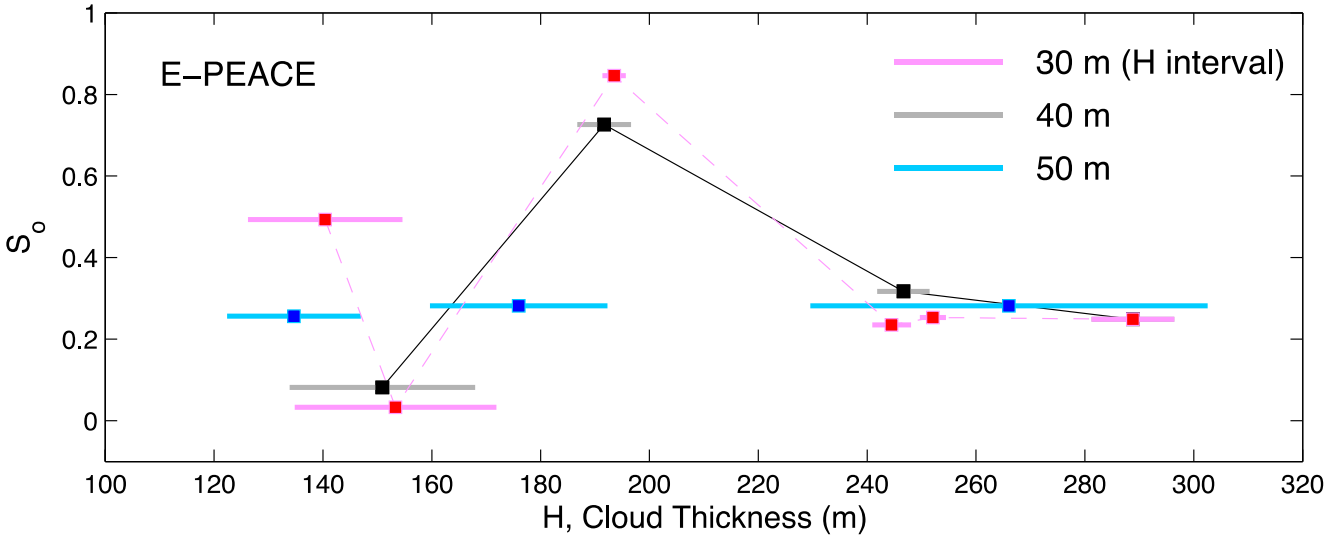

Figure C1. S_o is calculated with cloud data that are averaged over an e-folding time for E-PEACE. S_o calculated with three H intervals (Δ30 m, Δ40 m, and Δ50 m) are shown. Horizontal bar indicates ±1σ cloud thickness for a given H interval.

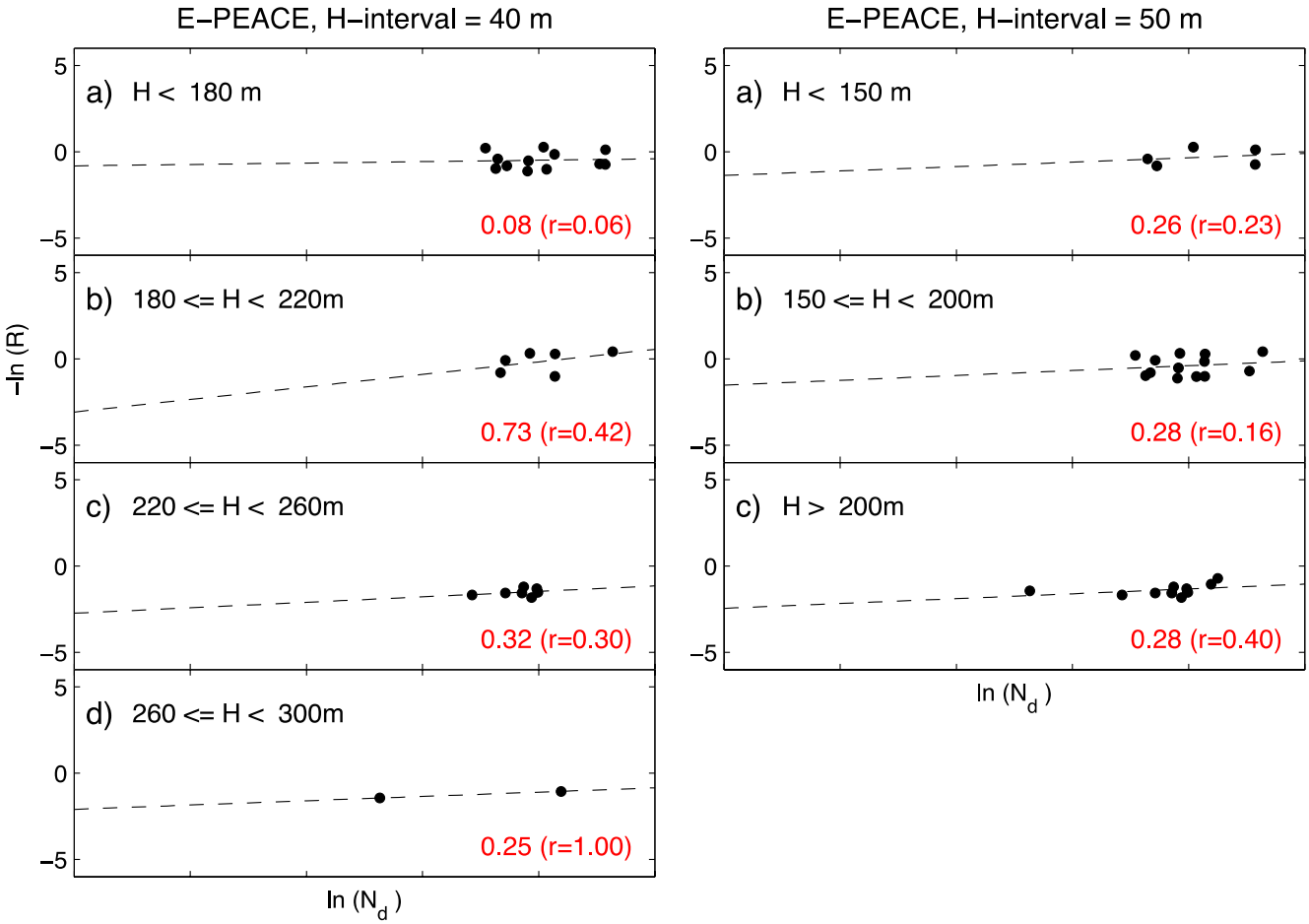

Figure C2. The ln (N_d) and –ln (R) diagrams with fixed H intervals: (left) ΔH=40 m, (right) ΔH=50 m.

5

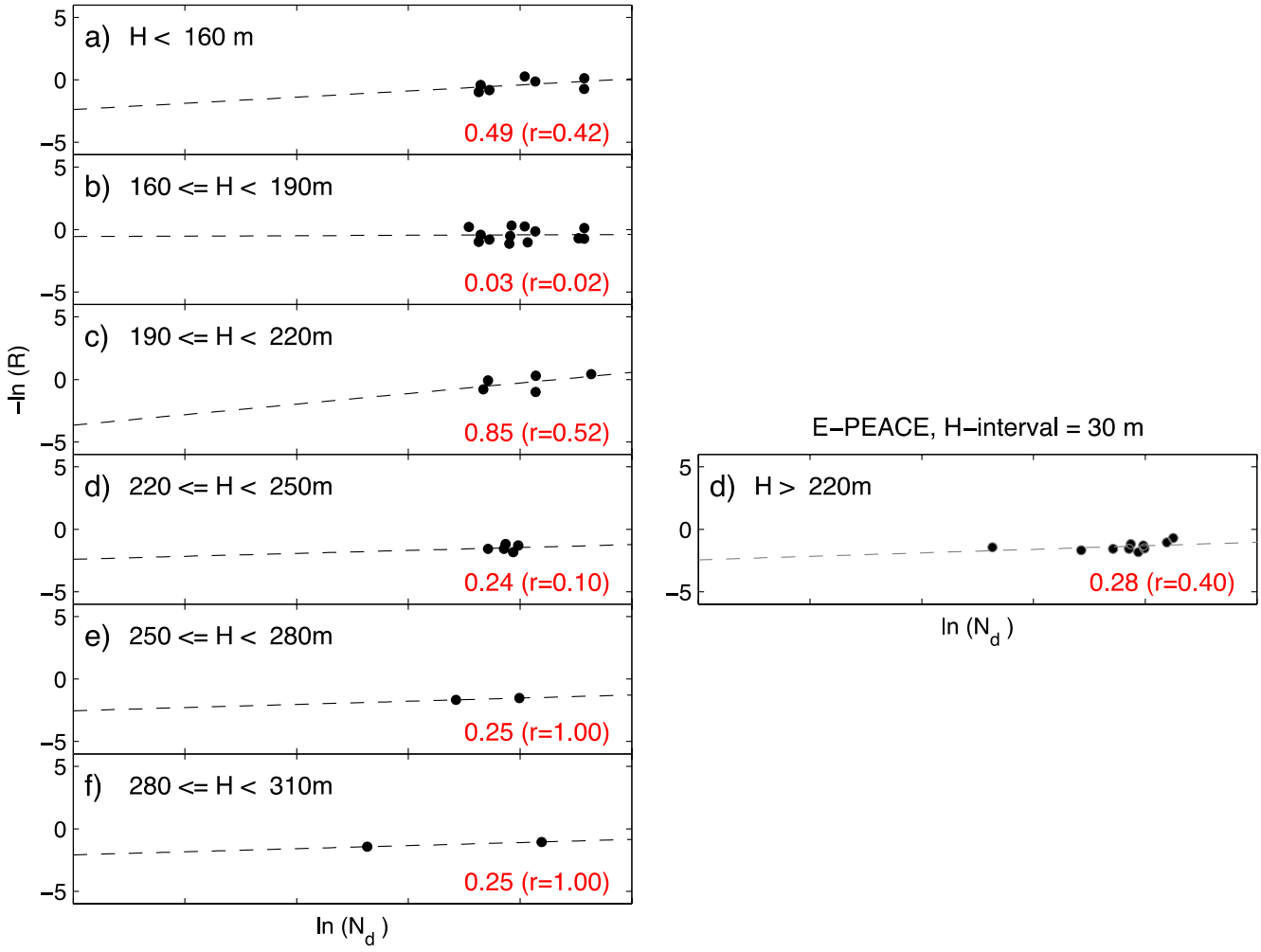

Figure C3. The ln (N_d) and –ln (R) diagrams with fixed H intervals (ΔH=30 m).

Acknowledgements

The authors gratefully acknowledge the crews of the CIRPAS Twin Otter for their assistance during these field campaigns. EJ acknowledges Chris Terai for his helpful discussion of the estimate of precipitation susceptibility. This study was funded by ONR Grants N000140810465, N00014-10-1-0811, N00014-16-1-2567, and NSF Grant AGS-1008848. We thank both reviewers for thoughtful suggestions and constructive criticism that have helped to improve the manuscript.

References

Bretherton, C. S., Wood, R., George, R. C., Leon, D., Allen, G., and Zheng, X.: Southeast Pacific stratocumulus clouds, precipitation and boundary layer structure sampled along 20 S during VOCALS-REx, Atmos. Chem. Phys., 10, 10639–10654, doi:10.5194/acp-10-10639-2010, 2010.

Comstock, K. K., Wood, R., Yuter, S. E., and Bretherton, C. S.: Reflectivity and rain rate in and below drizzling stratocumulus, Quart. J. Roy. Meteor. Soc., 130, 2891–2918, 2004.

Duong, H. T., Sorooshian, A., and Feingold, G.: Investigating potential biases in observed and modeled metrics of aerosol-cloud-precipitation interactions, Atmos. Chem. Phys., 11, 4027-4037, doi:10.5194/acp-11-4027-2011, 2011.

Feingold, G. and Siebert, H.: In Clouds in the Perturbed Climate System: Their Relationship to Energy Balance, Atmospheric Dynamics, and Precipitation, edited by: Heintzenberg, J. and Charlson, R. J., Stru¨ngmann Forum Reports, 2, Cambridge, MA: The MIT Press, 597, 2009.

Feingold, G., McComiskey, A., Rosenfeld, D., and Sorooshian, A.: On the relationship between cloud contact time and precipitation susceptibility to aerosol, J. Geophys. Res., 118, 10544–10554, 2013.

Gerber, H., Arends, B. G., and Ackerman, A. S.: A new microphysics sensor for aircraft use, Atmos. Res., 31, 235–252, 1994.

Gettelman, A., Morrison, H., Terai, C. R., and Wood, R.: Microphysical process rates and global aerosol–cloud interactions, Atmos. Chem. Phys., 13, 9855-9867, doi:10.5194/acp-13-9855-2013, 2013.

Intergovernmental Panel on Climate Change (IPCC): The Physical Science Basis. Contribution of Working Group I to the Fifth Assessment Report of the Intergovernmental Panel on Climate Change. Stocker, T.F., Qin, D., Plattner, G.-K., Tignor, M., Allen, S.K., Boschung, J., Nauels, A., Xia, Y., Bex, V. and Midgley, P.M. (eds.), Cambridge University Press, Cambridge, United Kingdom and New York, NY, USA, 2013.

Jiang, H., Feingold, G., and Sorooshian, A.: Effect of aerosol on the susceptibility and efficiency of precipitation in trade cumulus clouds, J. Atmos. Sci., 67, 3525–3540, 2010.

Jones, A., Roberts, D. L., Woodage, M. J., and Johnson, C. E.: Indirect sulphate aerosol forcing in a climate model with an interactive sulphur cycle, J. Geophys. Res., 106, 20,293–20,310, doi:10.1029/2000JD000089, 2001.

Jung, E.: Aerosol-Cloud-Precipitation Interactions in the Trade Wind Boundary Layer, PhD dissertation, 184pp, http://scholarlyrepository.miami.edu/oa_dissertations/900, 2012.

Jung, E., Albrecht, B. A., Feingold, G., Jonsson, H. H., Chuang, P., and Donaher, S. L.: Aerosols, Clouds, and Precipitation in the North-Atlantic Trades Observed During the Barbados Aerosol Cloud Experiment. Part I: Distributions and Variability, submitted to Atmos. Chem. Phys., ACP, 2016.

Jung, E., Albrecht, B. A., Prospero, J. M., Jonsson, H. H., and Kreidenweis, S. M.: Vertical structure of aerosols, temperature and moisture associated with an intense African dust event observed over the Eastern Caribbean, J. Geophys. Res., 118, 4623–4643. doi: 10.1002/jgrd.50352, 2013.

Jung, E., Albrecht, B. A., Jonsson, H. H., Chen, Y.-C., Seinfeld, J. H., Sorooshian, A., Metcalf, A. R., Song, S., Fang, M., and Russell, L. M.: Precipitation effects of giant cloud condensation nuclei artificially introduced into stratocumulus clouds, Atmos. Chem. Phys., 15, 5645-5658, doi:10.5194/acp-15-5645-2015, 2015.

Khairoutdinov, M., and Y. Kogan, Y.: A new cloud physics parameterization in a large-eddy simulation model of marine stratocumulus, Mon. Weather Rev., 128, 229–243, 2000.

Lee, G., and I. Zawadzki, I.: Variability of drop size distributions: time-scale dependence of the variability and its effects on rain estimation, J. Appl. Meteor. , 44, 241–255, doi:10.1175/JAM2183.1, 2005.

Leith, C. E.: The Standard Error of Time-Average Estimates of Climatic Means, J. Appl. Meteorl., 12, 1066–1069, doi:10.1175/1520-0450(1973)012<1066:TSEOTA>2.0.CO;2,1973.

Lu, M. -L., Sorooshian, A., Jonsson, H. H., Feingold, G., Flagan, R. C., and Seinfeld, J. H.: Marine stratocumulus aerosol-cloud relationships in the MASE-II experiment: Precipitation susceptibility in eastern Pacific marine stratocumulus, J. Geophys. Res., 114, D24203, doi:10.1029/2009JD012774, 2009.

Mann, J. A. L, Chiu, J. C., Hogan, R. J., O'Connor, E. J., L'Ecuyer, T. S., Stein, T. H. M., and Jefferson, A.: Aerosol impacts on drizzle properties in warm clouds from ARM Mobile Facility maritime and continental deployments, J. Geophys. Res., 119, doi:10.1002/2013JD021339, 2014.

Nuijens, L., Serikow, I., Hirsch, L., Lonitz, K., and Stevens, B.: The distribution and variability of low-level cloud in the North- Atlantic trades, Q. J. Roy. Meteorol. Soc., 140, 2364-2374, 2014.

Painemal, D., and Zuidema, P.: Assessment of MODIS cloud effective radius and optical thickness retrievals over the Southeast Pacific with VOCALS-REx in situ measurements, J. Geophys. Res., 116, D24206, doi:10.1029/2011JD016155, 2011.

Pawlowska, H. and Brenguier, J. L.: An observational study of drizzle formation in stratocumulus clouds for general circulation model (GCM) parameterizations, J. Geophys. Res., 108(D15), 8630, doi:10.1029/2002JD002679, 2003.

Rasch, P. J., and Kristjansson, J. E.: A comparison of the CCM3 model climate using diagnosed and predicted condensate parameterizations, J. Climate, 11, 1587–1614, 1998.

Rauber, R. M., Ochs III, H. T., Di Girolamo, L., Göke, S., Snod- grass, E., Stevens, B., Knight, C., Jensen, J. B., Lenschow, D. H., Rilling, R. A., Rogers, D. C., Stith, J. L., Albrecht, B. A., Zuidema, P., Blyth, A. M., Fairall, C. W., Brewer, W. A., Tucker, S., Lasher-Trapp, S. G., Mayol-Bracero, O. L., Vali, G., Geerts, B., Anderson, J. R., Baker, B. A., Lawson, R. P., Bandy, A. R., Thornton, D. C., Burnet, E., Brenguier, J-L., Gomes, L., Brown, P. R. A., Chuang, P., Cotton, W. R., Gerber, H., Heikes, B. G., Hudson, J. G., Kollias, P., Krueger, S. K., Nuijens, L., O'Sullivan, D. W., Siebesma, A. P., and Twohy, C. H.: Rain in shallow cu- mulus over the ocean, B. Am. Meteorol. Soc., 88, 1912–1928, 2007.

Rogers, R. R. and Yau, M. K.: A Short Course in Cloud Physics, Third Edition. International Series in Natural Philosophy, 290 pp, 1989.

Rosenfeld, D., Wang, H., and P. J. Rasch, P. J.: The roles of cloud drop effective radius and LWP in determining rain properties in marine stratocumulus, *Geophys. Res. Lett.,39,* L13801, doi:10.1029/2012GL052028, 2012.

Rotstayn, L. D., and Y. Liu, Y.: A smaller global estimate of the second indirect aerosol effect, Geophys. Res. Lett., 32, L05708, doi:10.1029/2004GL021922, 2005.

Russell, Lynn M., and Coauthors: Eastern Pacific Emitted Aerosol Cloud Experiment, Bull. Amer. Meteor. Soc., 94, 709–729. doi: http://dx.doi.org/10.1175/BAMS-D-12-00015.1, 2013.

Sorooshian, A., Feingold, G., Lebsock, M. D., Jiang, H., and Stephens, G.: On the precipitation susceptibility of clouds to aerosol perturbations, Geophys. Res. Lett., 36, L13803, doi:10.1029/2009GL038993, 2009.

Sorooshian, A., Feingold, G., Lebsock, M. D., Jiang, H., and Stephens, G.: Deconstructing the precipitation susceptibility construct: improving methodology for aerosol-cloud-precipitation studies, J. Geophys. Res., 115, D17201, doi:10.1029/2009JD013426, 2010.

Sorooshian, A., Prabhakar, G., Jonsson, H., Woods, R., Flagan, R. C., and J. H. Seinfeld, J. H.: On the presence of giant particles downwind of ships in the marine boundary layer, Geophys. Res. Lett., 42, doi:10.1002/2015GL063179, 2015.

Stevens, B, and Feingold, G.: Untangling aerosol effects on clouds and precipitation in a buffered system, Nature, 461, 607-613, 2009.

Takemura, T., Nozawa, T., Emori, S., Nakajima, T. Y., and Nakajima, T.: Simulation of climate response to aerosol direct and indirect effects with aerosol transport-radiation model, J. Geophys. Res., 110, D02202, doi:10.1029/2004JD005029, 2005.

Terai, C. R., Wood, R., Leon, D. C., and P. Zuidema, P.: Does precipitation susceptibility vary with increasing cloud thickness in marine stratocumulus?, Atmos. Chem. Phys., 12, 4567–4583, 2012.

Terai, C. R., Wood, R., and Kubar, T. L.: Satellite estimates of precipitation susceptibility in low-level marine stratiform clouds, J. Geophys. Res., 120, 8878-8889, 2015.

vanZanten, M. C., Stevens, B., Vali, G., and Lenschow, D. H.: Observations of drizzle in nocturnal marine stratocumulus, J. Atmos. Sci., 62, 88–106, 2005.

Wang, Z., Sorooshian, A., Prabhakar, G., Coggon, M. M., and Jonsson, H. H.: Impact of emissions from shipping, land, and the ocean on stratocumulus cloud water elemental composition during the 2011 E-PEACE Field Campaign, *Atmos. Environ., 89*, 570-580, doi.org/10.1016/j.atmosenv.2014.01.020, 2014.

Wonaschütz, A., Coggon, M., Sorooshian, A., Modini, R., Frossard, A. A., Ahlm, L., Mulmenstadt, J., Roberts, G. C., Russell, L. M., Dey, S., Brechtel, F. J., and Seinfeld, J. H.: Hygroscopic properties of smoke-generated organic aerosol particles emitted in the marine atmosphere, Atmos. Chem. Phys., 13, 9819-9835, 10.5194/acp-13-9819-2013, 2013.

Wood, R., Kubar, T. L., and Hartmann, D. L.: Understanding the Importantce of Microphysics and Macrophysics for Warm Rain in Marine Low Clouds. Part II: Heuristic Models of Rain Formation, J. Atmos. Sci., 66, 2973–2990, doi:10.1175/2009JAS3072.1, 2009.

Wood, R., Mechoso, C. R., Bretherton, C. S., Weller, R. A., Huebert, B., Straneo, F., Albrecht, B. A., Coe, H., Allen, G., Vaughan, G., Daum, P., Fairall, C., Chand, D., Gallardo Klenner, L., Garreaud, R., Grados, C., Covert, D. S., Bates, T. S., Krejci, R., Russell, L. M., de Szoeke, S., Brewer, A., Yuter, S. E., Springston, S. R., Chaigneau, A., Toniazzo, T., Minnis, P., Palikonda, R., Abel, S. J., Brown, W. O. J., Williams, S., Fochesatto, J., Brioude, J., and Bower, K. N.: The VAMOS Ocean-Cloud-Atmosphere-Land Study Regional Experiment (VOCALS-REx): goals, platforms, and field operations, Atmos. Chem. Phys., 11, 627-654, doi:10.5194/acp-11-627-2011, 2011.

Zheng, X., Albrecht, B., Jonsson, H. H., Khelif, D., Feingold, G., Minnis, P., Ayers, K., Chuang, P., Donaher, S., Rossiter, D., Ghate, V., Ruiz-Plancarte, J., and Sun-Mack, S.: Observations of the boundary layer, cloud, and aerosol variability in the southeast Pacific near-coastal marine stratocumulus during VOCALS-REx, Atmos. Chem. Phys., 11, 9943-9959, doi:10.5194/acp-11-9943-2011, 2011.

Zuidema, P., Leon, D., Pazmany, A., and Cadeddu, M.: Aircraft millimeter-wave passive sensing of cloud liquid water and water vapor during VOCALS-REx, Atmos. Chem. Phys., 12, 355-369, doi:10.5194/acp-12-355-2012, 2012.

Table 1. Dates used for this analysis during each experiment.

No.	VOCALS (Sc)	E-PEACE (Sc)	BACEX (Cu)	KWACEX (Cu)
Period	Oct.-Nov., 2008	July-Aug., 2011	Mar.-Apr., 2010	May, 2012
Location	Southeast Pacific Sc decks	Northeast Pacific Sc decks (California coast)	Barbados (Caribbean Sea and North Atlantic)	Key West (Caribbean Sea)
RF1	10/16 (2), 232 [29, 3]	7/19 [236, 2]	3/22 [39, 25]	5/22 (1st flight)
RF2	10/18 (3), 292±22 [152, 2]	7/21 [669, 144]	3/23 [92, 4]	5/22 (2nd flight)
RF3	10/19 (3) 323±16 [402, 28]	7/22 [610, 39]	3/24 [69, 1]	5/23
RF4	10/21 (1), 172 [376, 2]	7/23 [369, 20]	3/25 [68, 8]	5/24
RF5	10/22 (2), 224 [364, N/A]	7/26 [258, 131]	3/26 [28, 1]	-
RF6	10/26 (2), 208 [395, 11]	7/27 [702, 7]	3/29 [103, N/A]	-
RF7	10/27 (1), 142±38 [336, 2]	7/29 [731, 17]	3/30 [526, N/A]	-
RF8	10/30 (2), 213 [311, 170]	8/2 [395, 1]	3/31 [184, 2]	-
RF9	11/1 (4), 641 [146, 8]	8/3 [629, 1]	4/5 [138, 4]	-
RF10	11/9 (1), 164±18 [392, 44]	8/4 [378, 19]	4/7 [171, 7]	-
RF11	11/10 (1), 194±21 [279, 1]	8/5 [364, 93]	4/10 [133, 43]	-
RF12	11/12 (2), 249 [409, 66]	8/10 [721,1]	4/11 [123, 5]	-
RF13	11/13 (1), 183 [174, 35]	8/11 [10, 4]	-	-

*RF indicates the Research Flight. However, note that RFs from E-PEACE and VOCALS are not the same as RF from Russell et al. (2013) and Zheng et al. (2011), respectively.

*The daily mean cloud thickness (mean±1σ) for VOCALS are shown with the H category (the group number is shown in the parenthesis). See the details in section 2.4.

*Numbers inside brackets indicate e-folding time (seconds) of N_d and R

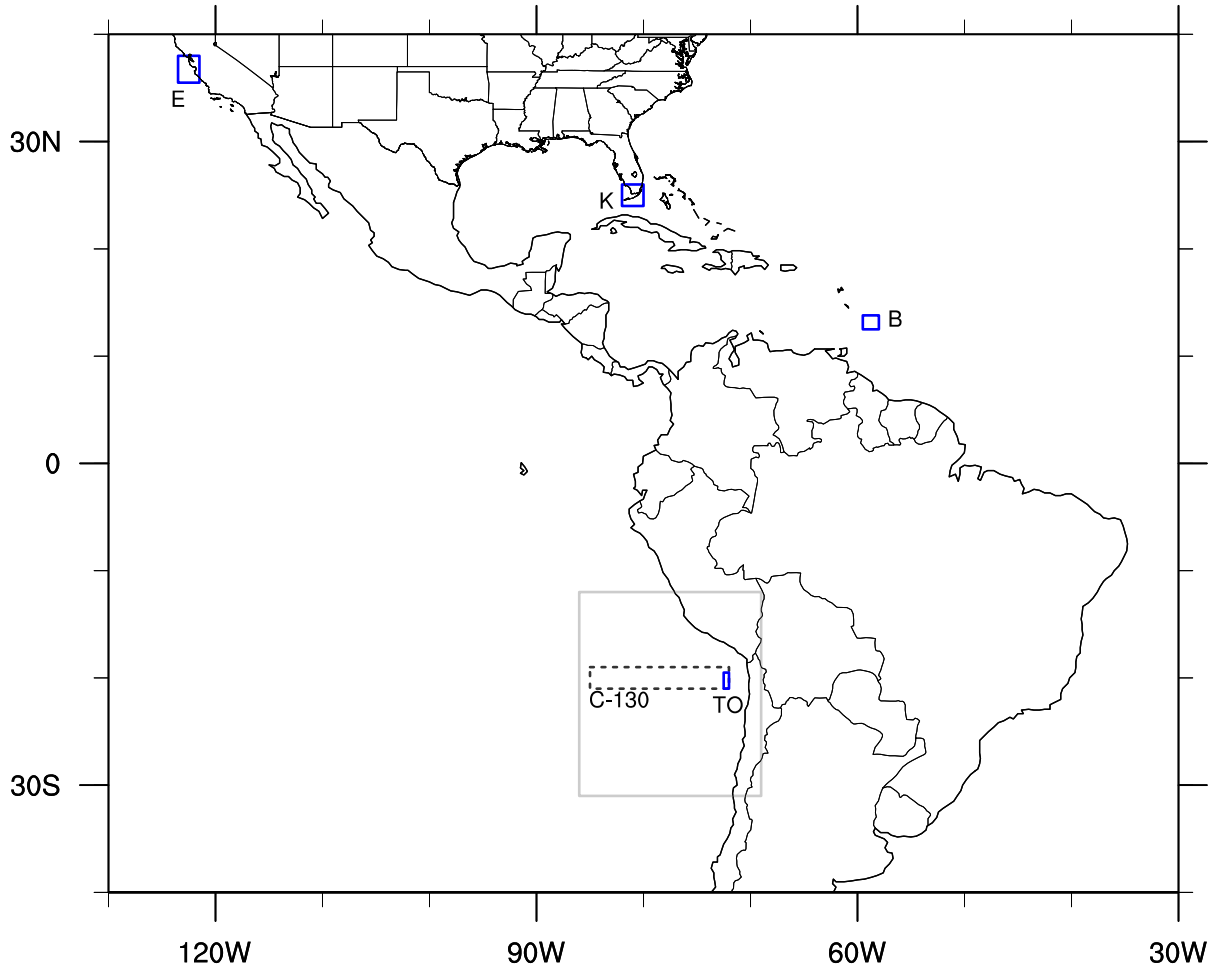

Figure 1: The geographical location of each field campaign (blue solid). E indicates E-PEACE, K indicates KWACEX, and B shows BACEX. The entire domain of VOCALS-REx is displayed as a solid grey box with domains of C-130 (dashed grey) and TO (solid blue) flights.

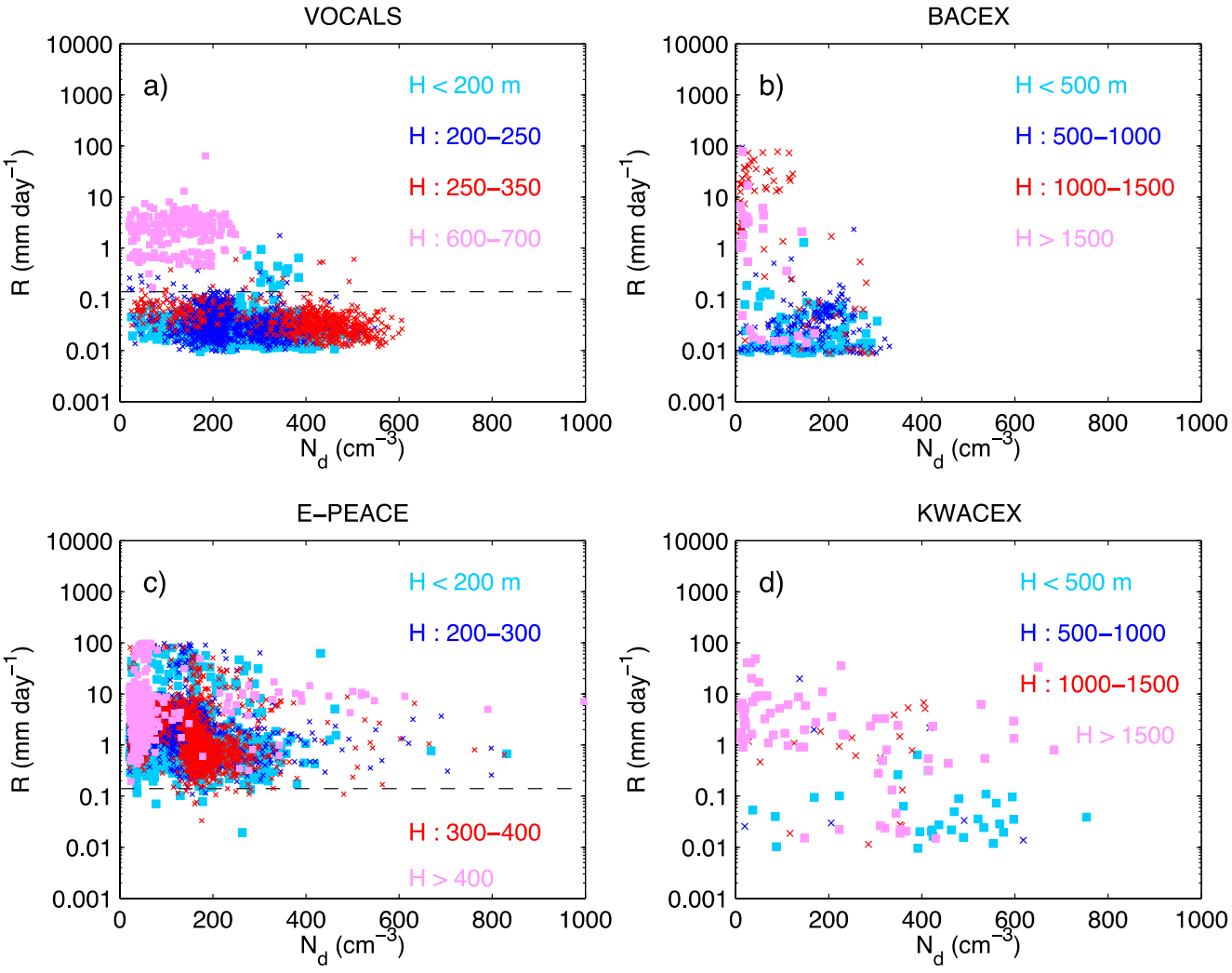

Figure 2: Scatter diagrams of cloud droplet number concentrations N_d and precipitation, R, for four field campaigns. Colors indicate cloud thickness H. The dashed line indicates an R value of 0.14 mm day^{-1}.

5

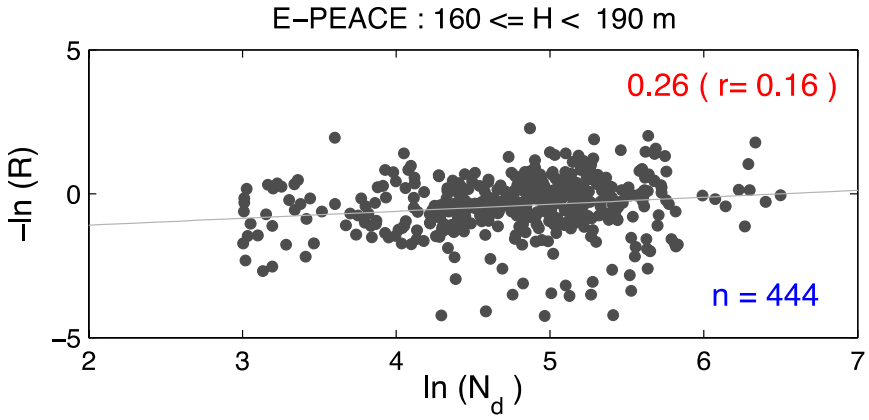

Figure 3: Examples of scatterplots used to calculate precipitation susceptibility S_o (i.e., the slope) for E-PEACE. Black dots indicate data points for an H interval between 160 m and 190 m. Numbers on the bottom right (blue) indicate the total number of data used. S_o and linear coefficient (r) values are shown in the upper right corner. Precipitation, R, increases downward in y ordinate, and N_d increases toward the right direction in x abscissa.

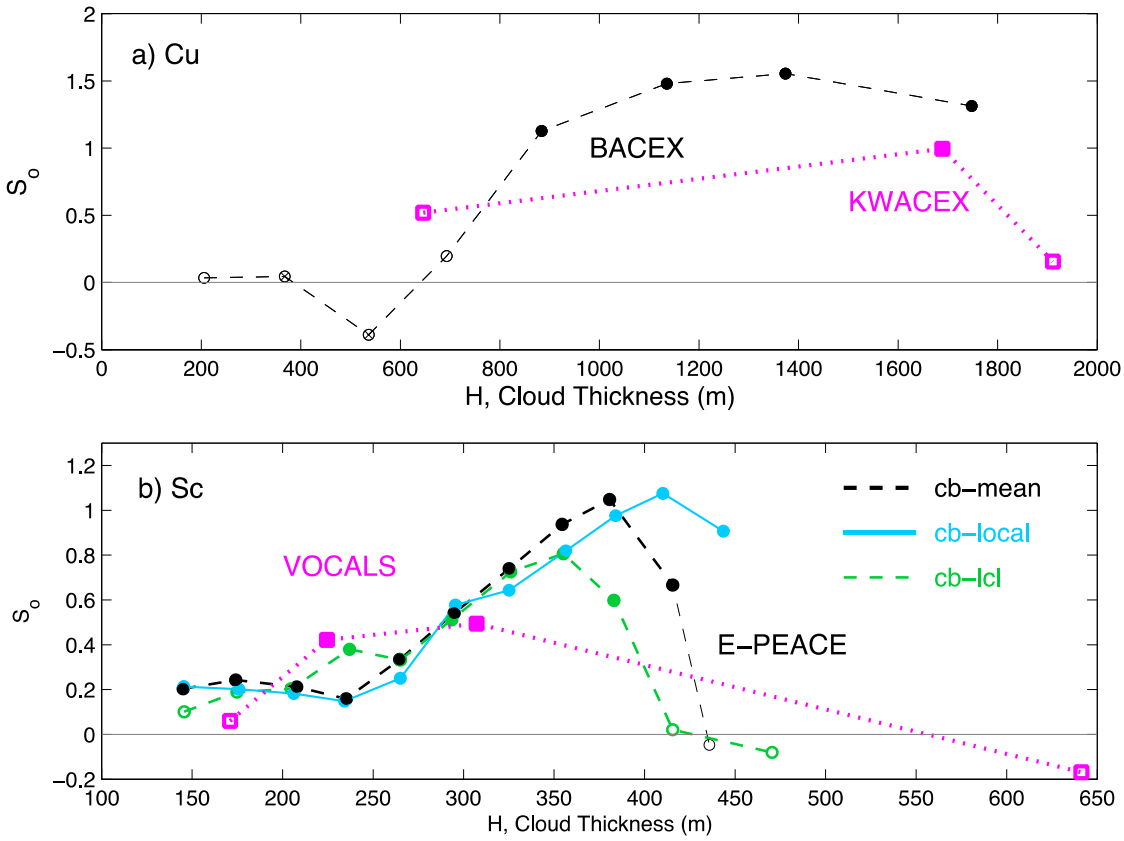

Figure 4: Precipitation susceptibility, S_o, estimated with aircraft measurements for (a) Cu (12 flights of BACEX and four flights of KWACEX) and (b) Sc (13 flights of E-PEACE and VOCALS-REx). E-PEACE S_o is estimated from (i) the cloud base height, which is identified using LCL (cb-lcl) and ii) from the vertical structures of LWCs (lowest height that the vertical gradient of LWC is the greatest) as the aircraft enters to the cloud deck to conduct the cloud-base level leg flight (cb-local), and (iii) from the averaged cloud-base heights from the nearby soundings and cb-local (cb-mean). Filled circles are statistically significant at 99 % confidence level. The number of data points used for S_o estimates and their statistical significance are shown in Table A2.

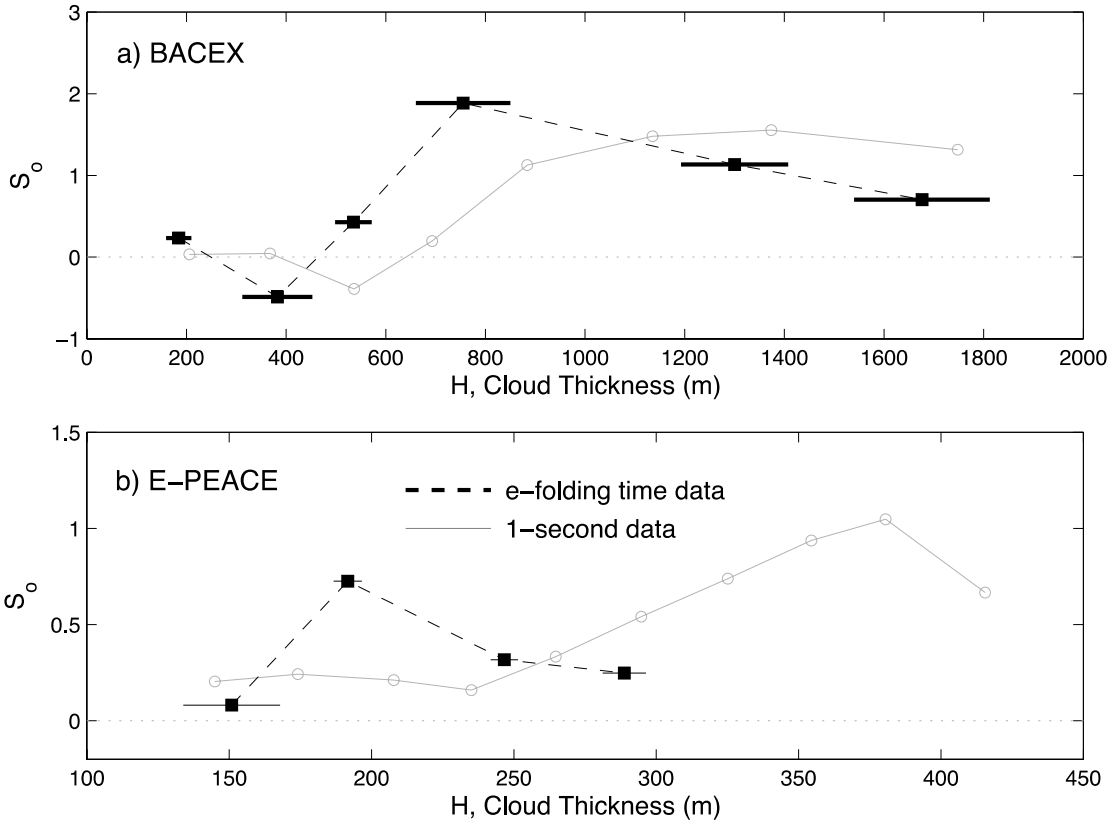

Figure 5. S_o estimated with aircraft measurements for (a) BACEX (Cu) and (b) E-PEACE (Sc). The 1-second data of individual flights are reduced by averaging over the e-folding time of N_d for each flight prior to the calculation.

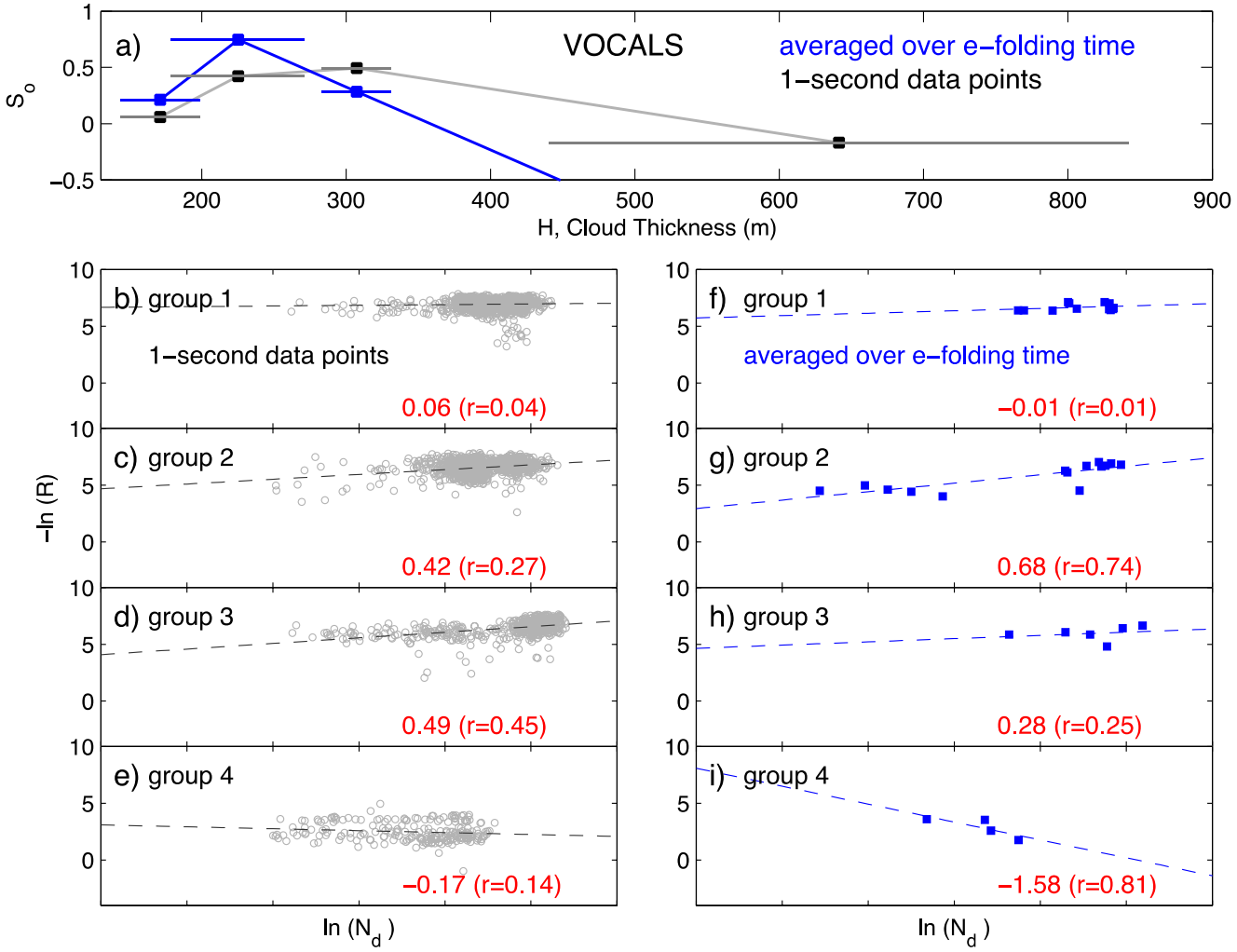

Figure 6. S_o for VOCALS TO flight is calculated with 1-second data (grey) and cloud data that are averaged over an e-folding time for each day (blue). The ln(N_d) and –ln(R) diagram is shown for each H interval. The horizontal bar in (a) indicates ±1σ. S_o is calculated for the cloud data in groups with similar H (shown in Table 1).

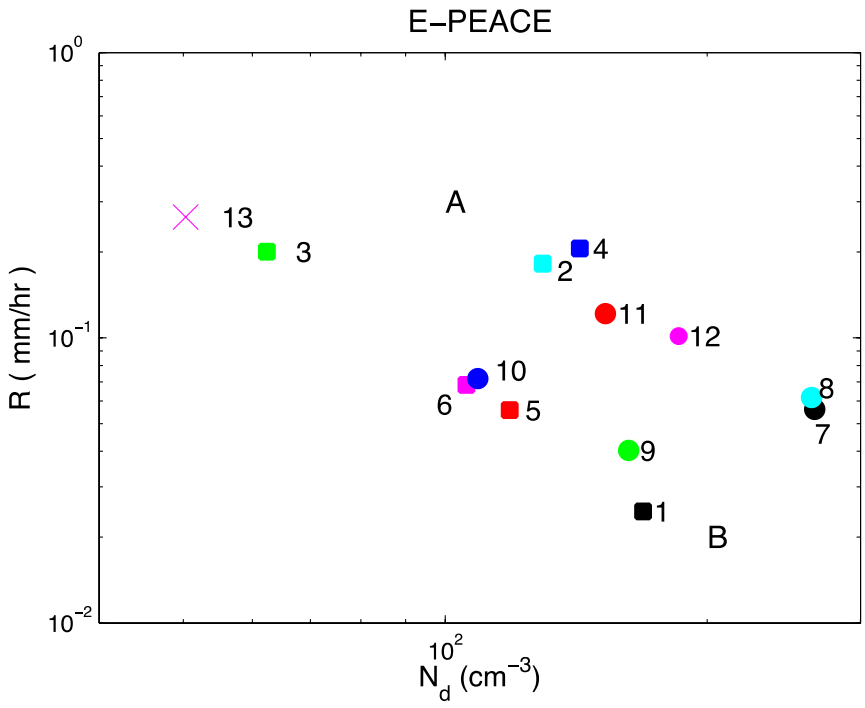

Figure 7. Daily mean values of N_d and R for the 13 E-PEACE flights. Numbers indicate the flight numbers shown in Table 1.

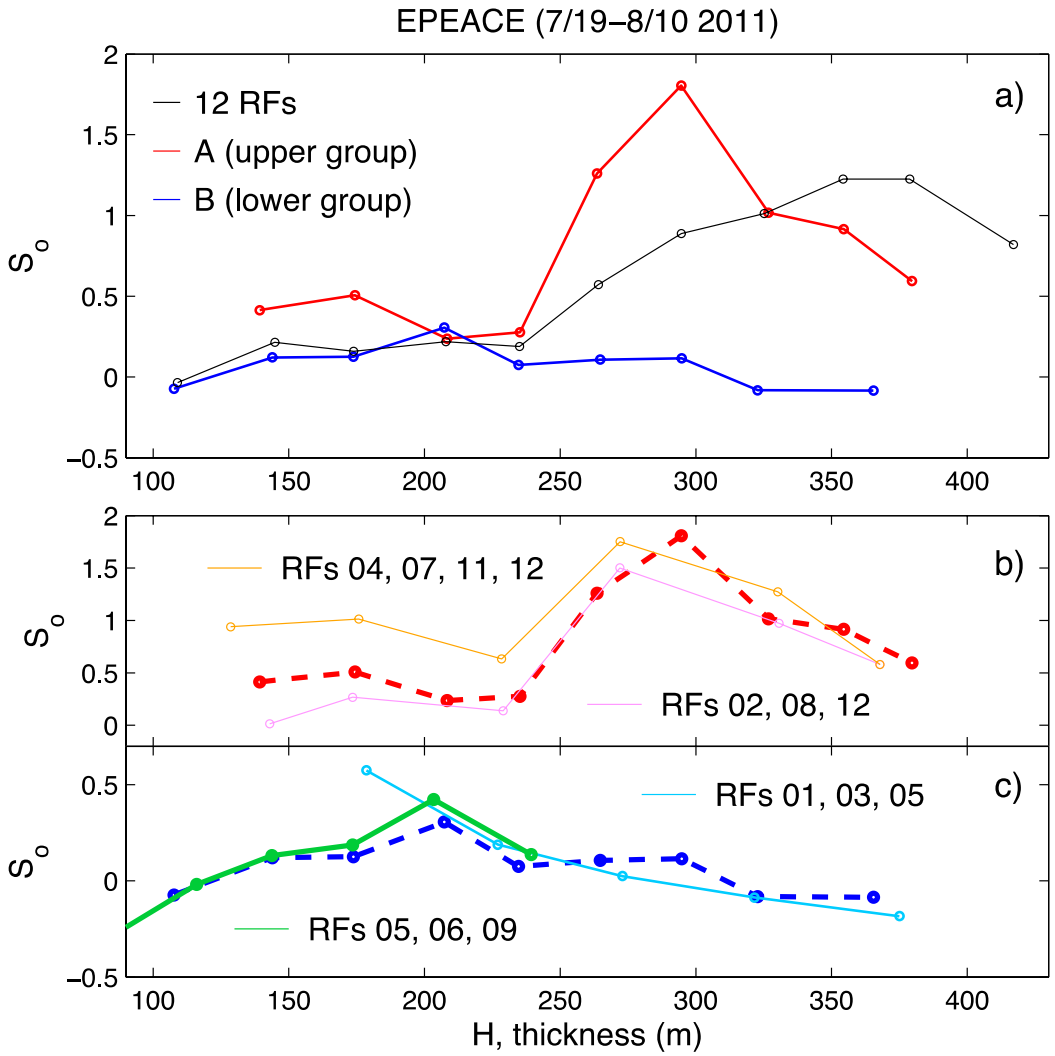

Figure 8. S_o as a function of cloud thickness for (a) 12 E-PEACE flights, for groups A and B shown in Fig. 7. (b) S_o calculated with randomly resampled RFs within groups (b) A and (b) B. RFs indicate Research Flights.

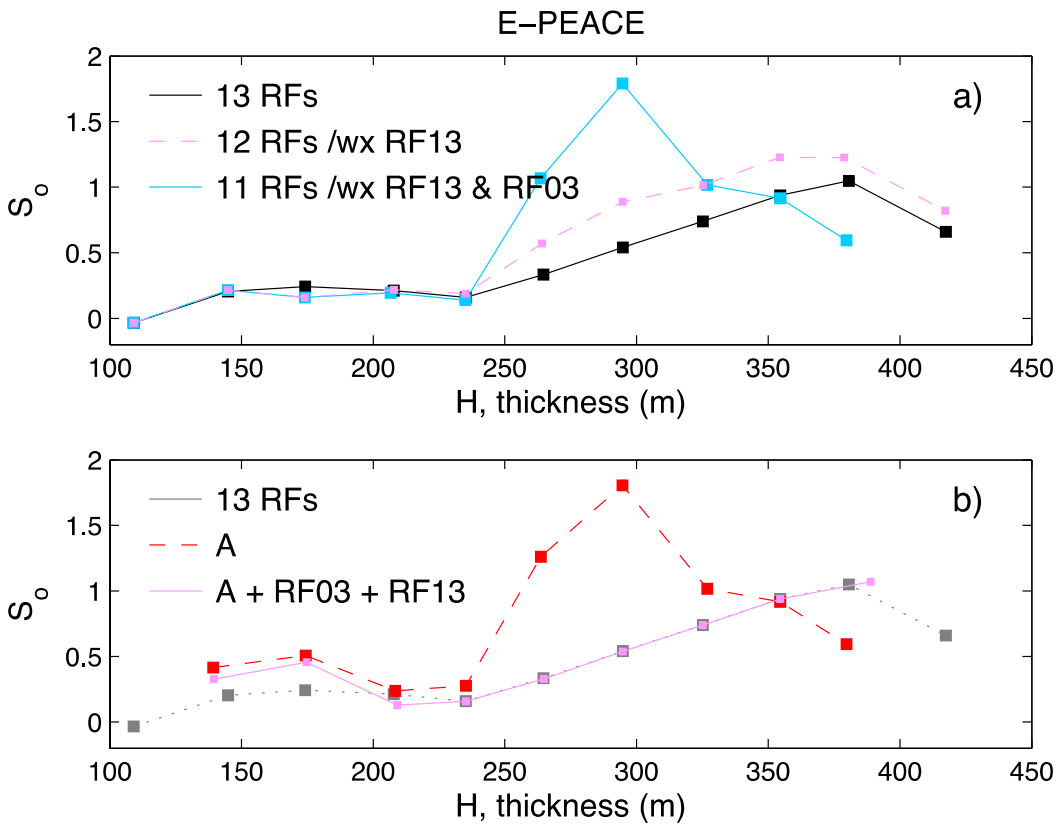

Figure 9. The effects of high precipitation (RF03 and RF13) on S_o estimates. (a) S_o calculated for 13 flights during E-PEACE in addition to when either, or both, RF03 and RF13 are excluded. RF03 and RF 13 are the flights of high precipitation rates. (b) S_o is calculated from group A with and without RF03 and RF13. R and N_d information for each flight is shown in Fig. 7.

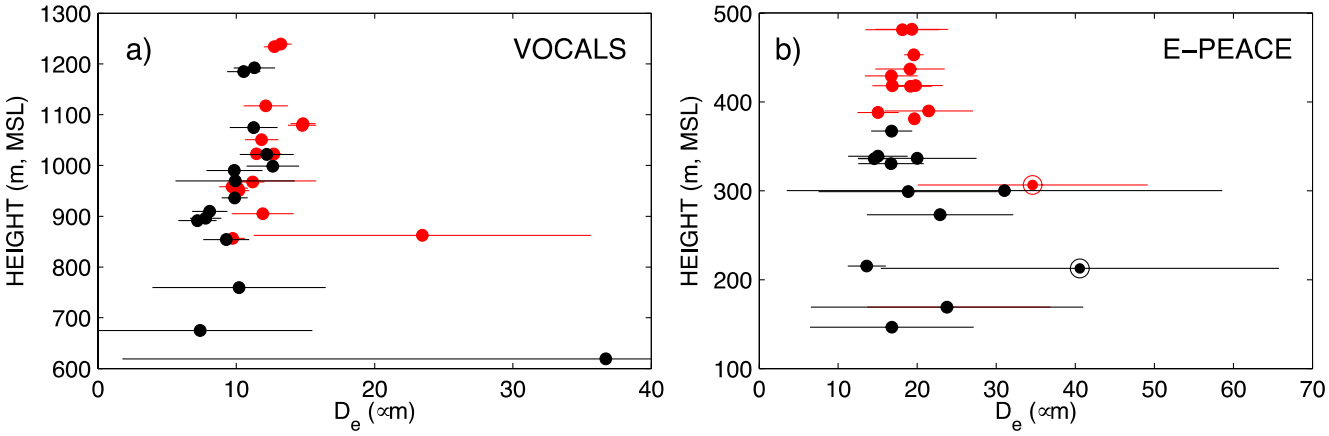

Figure 10: Distribution of effective diameters (mean ±1σ) for (a) VOCALS-TO flights and for (b) E-PEACE. Cloud droplets on 11 August are shown as double circles in Fig. 10(b).

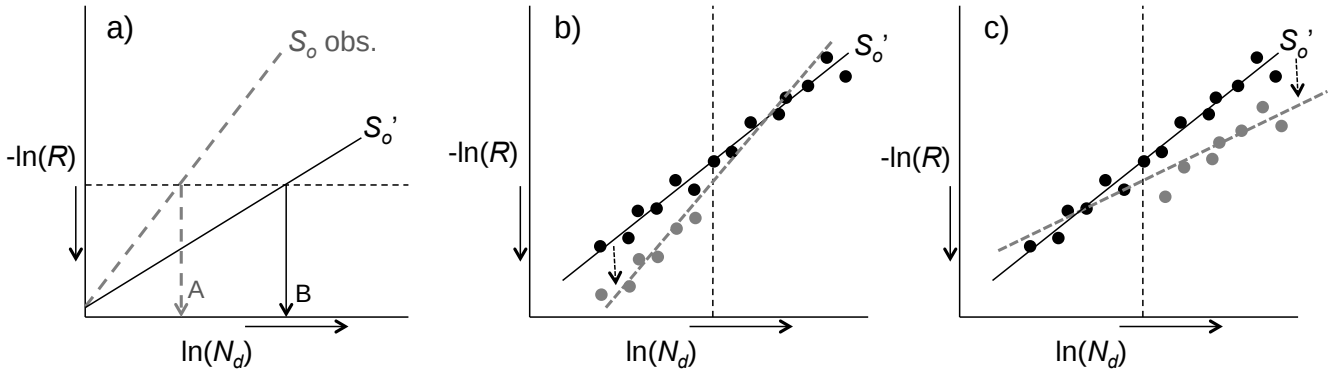

Figure 11: A visual description of (a) the effect of wet scavenging and (b-c) the impact of an increase in rainfall rate for a given range of N_d on the estimate of S_o. The solid line represents true (expected) S_o, whereas the dashed line indicates observed (or responded) S_o. The A and B in Fig. 11(a) indicate N_d that are supposed to be for the expected (theoretical) S_o and responded (observed) S_o, respectively. The black filled circles in (b-c) indicate the initial (or actual) data and the grey filled circles indicate newly adjusted (responded) data accordingly to the scenario. R increases downward on y ordinate and N_d increase toward the right direction on x abscissa.